Spectral and transport properties of a half-filled Anderson impurity coupled to phase-biased superconducting and metallic leads

Peter Zalom [1,*], Vladislav Pokorný [1,†], and Tomáš Novotný [2,‡]

[1]*Institute of Physics, Czech Academy of Sciences, Na Slovance 2, CZ-18221 Praha 8, Czech Republic*
[2]*Department of Condensed Matter Physics, Faculty of Mathematics and Physics, Charles University, Ke Karlovu 5,*
CZ-12116 Praha 2, Czech Republic

We derive and apply a general scheme for mapping a setup consisting of a half-filled single-level quantum dot coupled to one normal metallic and two superconducting phase-biased leads onto an ordinary half-filled single impurity Anderson model with single modified tunneling density of states. The theory allows for the otherwise unfeasible application of the standard numerical renormalization group and enables us to obtain phase-dependent local spectral properties as well as phase-dependent induced pairing and Josephson current. The resulting transport properties match well with the numerically exact continuous-time hybridization-expansion quantum Monte Carlo. For weakly coupled normal electrode, the spectral properties can be interpreted in terms of normal-electrode-broadened Andreev bound states with phase-dependent position analogous to the superconducting Anderson model, which coexist in the π-like phase with a Kondo peak whose phase-dependent Kondo temperature is extracted.

I. INTRODUCTION

Gradual advance in experimental techniques over the past decades enables to study electronic transport in increasingly sophisticated nanoscale systems with various, competing correlations. A prototype experiment typically includes a strongly interacting mesoscopic system attached to a reservoir with well-defined properties. In theory, the mesoscopic system is frequently described in terms of one or multiple quantum dots (QDs) in the Coulomb blockade regime while the reservoir consists of normal metallic and/or superconducting leads. Experimental realizations of such QDs include, for example, carbon nanotubes [1–10] or semiconductor nanowires [11–14].

The case of normal metallic electrodes attached to one QD can be modeled microscopically by the single-impurity Anderson model (SIAM) which is one of the most understood models in the many-body physics [15]. Here, free conduction electrons of the reservoir can completely or partially screen the magnetic doublet of QD depending on the parameters under the study. When the screening is effective, an emergent Kondo singlet becomes the ground state of the system [15]. The Kondo singlet is a coherent many-body state with logarithmic energy scaling that can only be fully understood by applying renormalization group (RG) techniques [16–18] or at least effective renormalization schemes [19,20].

Once superconducting correlations are considered in the reservoir, the electron transport is altered by the Andreev scattering on the interface between the leads and QD [21–25], but

it is still well described theoretically in terms of the Anderson impurity model with superconducting leads, denoted also as SCIAM [26]. For purely superconducting reservoirs, both the theoretical [27,28] and experimental [29] understanding is fairly complete. In particular, a sufficiently large gap depopulates electrons around the Fermi energy to such an extent that the screening cloud around the impurity becomes disrupted. The ground state of the system changes then from a singlet (effective screening at small sized gaps) to a doublet, which is an example of an impurity quantum phase transition (QPT). This so-called 0-π transition is accompanied by the reversal of the supercurrent, which is positive in the singlet and negative in the doublet phase [5,11,30]. At the transition, one also observes the crossing of the Andreev bound states (ABSs) at the Fermi energy.

Hybrid systems incorporating simultaneously normal as well as superconducting reservoirs, lead to even more intricate interplay of quantum correlation effects, where the understanding is limited both theoretically and experimentally [27,31–39]. In a simplest realization, one metallic and one superconducting lead have been studied experimentally in N-QD-S heterostructures [33]. From the theoretical perspective, such a problem is of only two-channel nature and thus well tractable by the numerical renormalization group (NRG) [31] which offers unbiased insights and thus complements the purely numerical quantum Monte Carlo (QMC) simulations with reliable spectral properties [34]. However, having just one superconducting lead does not allow superconducting phase difference across the QD. Consequently, such systems lack any supercurrent flow and no interplay of Kondo and Josephson effects takes place. Thus, the more interesting scenario includes one normal and two phase-biased superconducting leads. The resulting three-terminal structure is, however, beyond the reach of standard NRG since the

---

*zalomp@fzu.cz
†pokornyv@fzu.cz
‡tno@karlov.mff.cuni.cz

corresponding discretized reservoir corresponds to three spin dependent and mutually interconnected hopping chains. The standard NRG scheme has thus been so far employed only to two channel problems [35,36].

In the standard, computationally intractable approach to NRG [40], one would first discretize the bath of the three terminals. The resulting semi-infinite hopping chain would be then transformed via the Bogolyubov-Valatin transformation at each chain site. Subsequently, in the second step, particle-hole transformations on odd and even sites separately need to be carried out [35,36]. The resulting Wilson chain would, however, consist of three mutually interconnected spin-polarized chains which is beyond the present computational power [34]. To circumvent the problem, one may apply a general procedure of Ref. [41] or introduce suitable unitary transformations to diagonalize the problem [37–39]. The second approach has already been successfully applied to the hybrid normal-superconductor reservoir problem in the limit of infinite superconducting gap. Although the authors of Refs. [37–39] make explicit reference to the Wilson chains corresponding to discretized versions of the model under the study, as shown in the present paper, it is possible to limit the transformations in the case of half-filling [42] to just the local electrons of QD and map the infinite-gap model onto an ordinary asymmetric SIAM directly.

Generalizing the approach of Refs. [37–39], we are able to treat the present general three-terminal problem at the half-filling with finite superconducting gap and map it onto a single impurity Anderson model of fermions with tunneling density of states (TDOS) in the reservoir that corresponds to the standard one-channel-lead case tractable by NRG in the scheme of Ref. [43]. Since it is believed that such an approach is not feasible [44], we present the details of the transformation in Sec. II where also a detailed microscopic formulation of the problem is stated. In Sec. III, we proceed to the $\Delta \to \infty$ case treated previously in Refs. [37–39] and show that their approach is completely equivalent with ours when the half-filled case is considered. However, as opposed to Refs. [37–39], no reference to NRG discretization is required. Finally, in Sec. IV, the general three-terminal problem with finite superconducting gap is solved at the half-filling. To this end, the mapping of the finite-gap problem onto a single-channel SIAM with altered TDOS is performed. Subsequently, standard NRG approach of Ref. [43] is employed utilizing the NRG Ljubljana code [45]. Using the backwards transformations, all spectral and transport properties of the original three-terminal setup are then determined. The most important conclusions are summarized in Sec. V. Technical calculations regarding the transformation of the interaction term in Sec. II and the effect of the finite band width are discussed in the Appendices A and B, respectively. The comparison with QMC is shown in the Appendix C.

II. MAPPING ONTO SIAM-LIKE MODELS

A. Microscopic formulation

The hybrid three-terminal setup consists of a mesoscopic system modeled as a usual Anderson magnetic impurity connected to one normal metallic and two superconduct-

ing electrodes. The superconducting electrodes follow the Bardeen-Cooper-Schrieffer (BCS) theory with one lead referred to as the left (L) and the other one as the right (R), see Fig. 1. The total Hamiltonian of the system is then the sum of the dot Hamiltonian H_d, the Hamiltonian of the normal lead H_N, two BCS Hamiltonians for superconducting leads H_L and H_R, and three tunneling Hamiltonians $H_{T,\alpha}$ with $\alpha \in \{N, L, R\}$ which connect each lead separately to the dot. The constituent Hamiltonians read as

$$H_d = \sum_\sigma \varepsilon_d d_\sigma^\dagger d_\sigma + U d_\uparrow^\dagger d_\uparrow d_\downarrow^\dagger d_\downarrow, \tag{1}$$

$$H_\alpha = \sum_{\mathbf{k}\sigma} \varepsilon_{\mathbf{k}\alpha} c_{\alpha\mathbf{k}\sigma}^\dagger c_{\alpha\mathbf{k}\sigma}$$

$$- \Delta_\alpha \sum_{\mathbf{k}} (e^{i\varphi_\alpha} c_{\alpha\mathbf{k}\uparrow}^\dagger c_{\alpha-\mathbf{k}\downarrow}^\dagger + \text{H.c.}), \tag{2}$$

$$H_{T,\alpha} = \sum_{\mathbf{k}\sigma} (V_{\alpha\mathbf{k}}^* c_{\alpha\mathbf{k}\sigma}^\dagger d_\sigma + V_{\alpha\mathbf{k}} d_\sigma^\dagger c_{\alpha\mathbf{k}\sigma}), \tag{3}$$

where $c_{\alpha\mathbf{k}\sigma}^\dagger$ creates an electron of spin $\sigma \in \{\uparrow, \downarrow\}$ and quasi-momentum $\mathbf{k}$ in the lead α while $c_{\alpha\mathbf{k}\sigma}$ annihilates it. In analogy, $d_\sigma^\dagger$ creates a dot electron of spin σ while d_σ annihilates it. The QD is characterized by the Coulomb repulsion U and the level energy ε_d which in the most general case is arbitrary but we will later concentrate only at $\varepsilon_d = -U/2$. The QD hybridizes with the leads via $V_{\alpha\mathbf{k}}$ and the gap parameter vanishes in the normal lead, thus $\Delta_N = 0$.

In all our calculations we use dimensionless units with $\hbar = 1$ and $e = 1$. Moreover, we focus on a generic case with a constant TDOS with a finite half-bandwidth B

$$\Gamma_\alpha(\omega) = \pi \sum_{\mathbf{k}} |V_{\alpha\mathbf{k}}|^2 \delta(\omega - \varepsilon_{\mathbf{k}\alpha}) = \Gamma_\alpha \Theta(B^2 - \omega^2), \tag{4}$$

which also defines the tunneling rates Γ_α. We concentrate on the case with symmetric coupling to the superconducting leads $\Gamma_L = \Gamma_R \equiv \Gamma_S/2$ as any asymmetric case $\Gamma_L \neq \Gamma_R$ can be obtained from the symmetric one using the procedure described in Ref. [46].

We also restrict to situations with the same gap parameters in both superconducting leads $\Delta_L = \Delta_R \equiv \Delta$ as this is a typical situation in an experiment. Concerning the BCS phase parameters φ_L and φ_R, as in any Josephson junction physical observables can only depend on the phase difference $\varphi = \varphi_L - \varphi_R$ and not on their individual values, i.e. they must be invariant with respect to a global phase shift $\varphi_{L,R} \to \varphi_{L,R} + \varphi_s$ which is a manifestation of the gauge invariance [28]. Therefore, we are free to choose a convenient symmetric phase-drop setup with $\varphi_L = -\varphi_R = \varphi/2$ in what follows.

The Hamiltonians of all three leads are quadratic due to the standard noninteracting assumption. Consequently, the lead electrons can be integrated out to obtain a genuine one channel impurity problem. To this end, it is advantageous to reformulate Eqs. (1)–(3) using the Nambu formalism.

B. Hamiltonian in the Nambu basis

Nambu formalism represents a convenient way of rearranging Hamiltonians involving BCS superconductivity in a way where all the lead electrons are treated on an equal footing. To this end, let us combine the spin up and spin down component
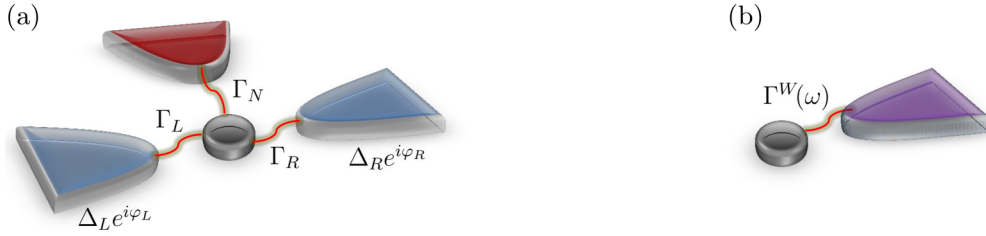
FIG. 1. (a) Scheme of Y-shaped three-terminal junction where a QD (black disk) couples via the hybridization strength Γ_N to one normal electrode (red pointed teardrop) and the left (L) and right (R) superconducting electrodes (blue pointed teardrops) which are phase-biased by $\varphi = \varphi_L - \varphi_R$. The BCS leads hybridize with quantum dot with strengths Γ_L and Γ_R, respectively, and are considered here as having the same BCS gap parameter $\Delta_L = \Delta_R \equiv \Delta$. (b) Equivalent scheme consisting of one-terminal reservoir containing Bogolyubov-like quasiparticles (purple pointed teardrop) which are hybridized with the QD via a structured hybridization function $\Gamma^W(\omega)$. In Sec. II C we show that by employing $\Gamma^W(\omega)$ according to Eq. (41) the schemes (a) and (b) may be in terms of spectral properties mapped onto each other at the half-filling. To obtain transport properties corresponding to the Y-shaped geometry of panel (a) transformations according to Sec. IV C are required.

of the corresponding fields describing the c electrons into spinors

$$C_{\alpha\mathbf{k}}^{\dagger} = (c_{\alpha\mathbf{k}\uparrow}^{\dagger}, c_{\alpha-\mathbf{k}\downarrow}), \tag{5}$$

with $\alpha \in \{N, L, R\}$, while the spinor D of the dot electrons d is constructed in complete analogy as

$$D^{\dagger} = (d_{\uparrow}^{\dagger}, d_{\downarrow}). \tag{6}$$

Under the standard BCS assumption $\varepsilon_{\mathbf{k}\alpha} = \varepsilon_{-\mathbf{k}\alpha}$ and with a convenient choice of real tunnel couplings $V_{\alpha\mathbf{k}} = V_{\alpha\mathbf{k}}^* = V_{\alpha-\mathbf{k}}$, the Hamiltonians (2) and (3) apart from possible unimportant constant energy shifts then become

$$H_{\alpha} = \sum_{\mathbf{k}} C_{\alpha\mathbf{k}}^{\dagger} \mathbb{E}_{\alpha\mathbf{k}} C_{\alpha\mathbf{k}}, \tag{7}$$

$$H_{T,\alpha} = \sum_{\mathbf{k}} (D^{\dagger} \mathbb{V}_{\alpha\mathbf{k}} C_{\alpha\mathbf{k}} + C_{\alpha\mathbf{k}}^{\dagger} \mathbb{V}_{\alpha\mathbf{k}} D), \tag{8}$$

with

$$\mathbb{E}_{\alpha\mathbf{k}} = -\Delta_{\alpha} C_{\alpha}\sigma_x + \Delta_{\alpha} S_{\alpha}\sigma_y + \varepsilon_{\mathbf{k}\alpha}\sigma_z, \tag{9}$$

$$\mathbb{V}_{\alpha\mathbf{k}} = V_{\alpha\mathbf{k}} \sigma_z, \tag{10}$$

where σ_i, $i \in \{x, y, z\}$, are the Pauli matrices while $C_{\alpha} \equiv \cos\varphi_{\alpha}$, $S_{\alpha} \equiv \sin\varphi_{\alpha}$. The blackboard bold font is from now on used to distinguish matrices from scalars.

Before applying the Nambu formalism to the Hamiltonian (1), let us first separate it into a quadratic part,

$$H_{d,0} = \sum_{\sigma} \varepsilon_d d_{\sigma}^{\dagger} d_{\sigma} + \frac{U}{2} D^{\dagger}(\sigma_x + \sigma_z)D$$

$$= D^{\dagger} \mathbb{E}_d D, \tag{11}$$

with

$$\mathbb{E}_d = \frac{U}{2}\sigma_x + \left(\frac{U}{2} + \varepsilon_d\right)\sigma_z, \tag{12}$$

and a mixed quadratic and quartic interaction part

$$H_U = U d_{\uparrow}^{\dagger} d_{\uparrow} d_{\downarrow}^{\dagger} d_{\downarrow} - \frac{U}{2} D^{\dagger}(\sigma_x + \sigma_z)D. \tag{13}$$

The advantage of this nonstandard partitioning will be discussed in Sec. II C.

Taking together, in the Nambu formalism the noninteracting quadratic part of the present problem spanned by the D and C spinors reads as

$$H_0 = H_{d,0} + \sum_{\alpha} (H_{\alpha} + H_{T,\alpha}), \tag{14}$$

while the modified interaction part H_U is given by Eq. (13).

C. Bogolyubov-Valatin transformations in the space of local electrons

Let us now study the effect of unitary transformations $\mathbb{T}$ and $\tilde{\mathbb{T}}_{\alpha}$ onto the spinors D and C_{α}, respectively. We introduce the spinors W and $\tilde{C}$ via

$$\mathbb{T}D \equiv W, \quad D^{\dagger}\mathbb{T}^{\dagger} \equiv W^{\dagger}, \tag{15}$$

$$\tilde{\mathbb{T}}_{\alpha} C_{\alpha\mathbf{k}} \equiv \tilde{C}_{\alpha\mathbf{k}}, \quad C_{\alpha\mathbf{k}}^{\dagger} \tilde{\mathbb{T}}_{\alpha}^{\dagger} \equiv \tilde{C}_{\alpha\mathbf{k}}^{\dagger}. \tag{16}$$

At this point, we consider no other constraints on the transformations $\mathbb{T}$, $\tilde{\mathbb{T}}_{\alpha}$ except of unitarity so that the many-body energy spectra of the problem remain invariant. On the other hand, such transformations may crucially affect the form of the one-particle operators in the corresponding noninteracting Hamiltonians thus allowing for computationally more suitable noninteracting Green functions and/or self-energy contributions from the integrable degrees of freedom for the problem under the study.

The effect of the transformations $\mathbb{T}$ and $\tilde{\mathbb{T}}_{\alpha}$ on the quadratic part $H_{d,0}$ reads as

$$H_{d,0} = W^{\dagger}(\mathbb{T}\mathbb{E}_d\mathbb{T}^{\dagger})W, \tag{17}$$

while the tunneling Hamiltonians change as

$$H_{T,\alpha} = \sum_{\mathbf{k}} W^{\dagger}(\mathbb{T}\mathbb{V}_{\alpha\mathbf{k}}\tilde{\mathbb{T}}_{\alpha}^{\dagger})\tilde{C}_{\alpha\mathbf{k}} + \sum_{\mathbf{k}} \tilde{C}_{\alpha\mathbf{k}}^{\dagger}(\tilde{\mathbb{T}}_{\alpha}\mathbb{V}_{\alpha\mathbf{k}}\mathbb{T}^{\dagger})W. \tag{18}$$

The kinetic Hamiltonians are affected only by the transformations $\tilde{\mathbb{T}}_{\alpha}$ as they involve no operators of the local electrons:

$$H_{\alpha} = \sum_{\mathbf{k}} \tilde{C}_{\alpha\mathbf{k}}^{\dagger}(\tilde{\mathbb{T}}_{\alpha}\mathbb{E}_{\alpha\mathbf{k}}\tilde{\mathbb{T}}_{\alpha}^{\dagger})\tilde{C}_{\alpha\mathbf{k}}. \tag{19}$$

Since the noninteracting ($U = 0$) Hamiltonian is quadratic we can easily obtain the retarded Green function $\mathbb{G}_0^W(\omega^+)$ [47]

which corresponds to the W spinors. Employing the equation of motion technique for the Green functions in an exact analogy to Ref. [48], we introduce an infinite-dimensional vector

$$\Psi^\dagger = (W^\dagger, \ \tilde{C}^\dagger_{N\mathbf{k}}, \ \tilde{C}^\dagger_{L\mathbf{k}}, \ \tilde{C}^\dagger_{R\mathbf{k}}), \quad (20)$$

where Ψ is its Hermitian conjugate and the spinors $\tilde{C}^\dagger_{\alpha\mathbf{k}}$ are understood to be repeated in $\Psi^\dagger$ for all possible quasimomenta of lead electrons. This allows us to rearrange the noninteracting Hamiltonian as

$$H_0 = \Psi^\dagger \mathbb{E}^W \Psi, \quad (21)$$

with

$$\mathbb{E}^W = \begin{pmatrix} \mathbb{T}\mathbb{E}_d\mathbb{T}^\dagger & \mathbb{T}\mathbb{V}_{N\mathbf{k}}\tilde{\mathbb{T}}^\dagger_N & \mathbb{T}\mathbb{V}_{L\mathbf{k}}\tilde{\mathbb{T}}^\dagger_L & \mathbb{T}\mathbb{V}_{R\mathbf{k}}\tilde{\mathbb{T}}^\dagger_R \\ \tilde{\mathbb{T}}_N\mathbb{V}_{L\mathbf{k}}\mathbb{T}^\dagger & \tilde{\mathbb{T}}_N\mathbb{E}_{N\mathbf{k}}\tilde{\mathbb{T}}^\dagger_N & 0 & 0 \\ \tilde{\mathbb{T}}_L\mathbb{V}_{L\mathbf{k}}\mathbb{T}^\dagger & 0 & \tilde{\mathbb{T}}_L\mathbb{E}_{L\mathbf{k}}\tilde{\mathbb{T}}^\dagger_L & 0 \\ \tilde{\mathbb{T}}_R\mathbb{V}_{R\mathbf{k}}\mathbb{T}^\dagger & 0 & 0 & \tilde{\mathbb{T}}_R\mathbb{E}_{R\mathbf{k}}\tilde{\mathbb{T}}^\dagger_R \end{pmatrix}, \quad (22)$$

where the upper index W was introduced to clearly distinguish the underlying spinor basis W for the formulation of the infinite-dimensional matrix $\mathbb{E}^W$.

In general, the noninteracting problem can be solved by finding the retarded Green function $\mathbb{G}_0(\omega^+)$ where $\omega^+ \equiv \omega + i\eta$ while ω is a real frequency and η is an infinitesimally small positive number. To this end, standard equation of motion technique formulated in the matrix form requires one to solve the resolvent equation $\mathbb{G}_0(\omega^+) = (\omega^+\mathbb{1} - \mathbb{H}_0)^{-1}$ with $\mathbb{1}$ being the unit matrix. However, for the present problem we only need to obtain the solution for the local Green function of the dot electrons which corresponds the left upper 2×2 block of expression (22). Employing the partitioning scheme of Ref. [48], we obtain the local retarded Green function $\mathbb{G}^W_0(\omega^+)$ in the spinor basis W directly as

$$\mathbb{G}^W_0(\omega^+) = (\omega^+\mathbb{1} - \mathbb{T}\mathbb{E}_d\mathbb{T}^\dagger - \mathbb{T}\Sigma^D\mathbb{T}^\dagger)^{-1}, \quad (23)$$

with

$$\Sigma^D(\omega^+) = \sum_{\alpha\mathbf{k}} \mathbb{V}_{\alpha\mathbf{k}}\tilde{\mathbb{T}}^\dagger_\alpha(\omega^+\mathbb{1} - \tilde{\mathbb{T}}_\alpha\mathbb{E}_{\alpha\mathbf{k}}\tilde{\mathbb{T}}^\dagger_\alpha)^{-1}\tilde{\mathbb{T}}_\alpha\mathbb{V}_{\alpha\mathbf{k}}$$

$$= \sum_{\alpha\mathbf{k}} \mathbb{V}_{\alpha\mathbf{k}}(\omega^+\mathbb{1} - \mathbb{E}_{\alpha\mathbf{k}})^{-1}\mathbb{V}_{\alpha\mathbf{k}}, \quad (24)$$

which thus represents the self-energy contribution from the leads expressed with respect to the spinor basis D (as denoted by the upper index D). Moreover, one may also obtain the self-energy contribution Σ^W as

$$\Sigma^W(\omega^+) = \mathbb{T}\Sigma^D(\omega^+)\mathbb{T}^\dagger, \quad (25)$$

which not only defines $\Sigma^W(\omega^+)$, but also gives us the transformation rule to easily interchange the spinor bases D and W when required. By exploiting the unitarity of $\mathbb{T}$, we may also extract an analogous transformation rule for the noninteracting retarded Green functions

$$\mathbb{G}^W_0(\omega^+) = \mathbb{T}(\omega^+\mathbb{1} - \mathbb{E}_d - \Sigma^D)^{-1}\mathbb{T}^\dagger = \mathbb{T}\mathbb{G}^D_0(\omega^+)\mathbb{T}^\dagger, \quad (26)$$

which yields also the definition of the noninteracting ($U = 0$) retarded Green function with respect to the spinor basis D.

Clearly, in both bases the effect of the leads is fully integrated out and only enters the $\mathbb{G}^W_0(\omega^+)$ and $\mathbb{G}^D_0(\omega^+)$ via the corresponding self-energy contributions $\Sigma^W(\omega^+)$ and $\Sigma^D(\omega^+)$, respectively. Green function as well as the self-energy contributions in different bases relate to each other via the local dot transformation $\mathbb{T}$ since the transformations $\tilde{\mathbb{T}}_\alpha$ are canceled out in Eqs. (25) and (26).

It is now our aim to construct a suitable transformation $\mathbb{T}$, so that the self-energy contribution Σ^W is diagonal. To this end, we first perform all summations in Eq. (24), which is quite straightforward with details given in the Appendix B. The resulting expression for $\Sigma^D(\omega^+)$ has the following matrix structure:

$$\Sigma^D(\omega^+) = \Sigma^D_n(\omega^+)\mathbb{1} + \Sigma^D_a(\omega^+)\sigma_x, \quad (27)$$

where $\Sigma^D_n(\omega)$ and $\Sigma^D_a(\omega)$ are functions of frequency with for now unimportant form given in the Appendix B. We insert now $\Sigma^D(\omega^+)$ back into Eq. (26) to obtain the matrix structure of $(\mathbb{G}^D_0)^{-1}$. We first concentrate exclusively on the half-filled case where $(\mathbb{G}^D_0)^{-1}$ has a much simpler structure. Afterwards, the more general $\varepsilon_d \neq -U/2$ case is inspected.

At the half-filling the diagonal part of $(\mathbb{G}^D_0)^{-1}$ is only proportional to the unit matrix $\mathbb{1}$ which remains unaltered under unitary transformation. On the other hand, the off-diagonal parts of Σ^D and $\mathbb{E}_d$ are both proportional to σ_x and may thus be simultaneously diagonalized by enforcing the condition $\mathbb{T}\sigma_x\mathbb{T}^\dagger = \pm\sigma_z$ onto the transformation $\mathbb{T}$. The resulting noninteracting Green function $\mathbb{G}^W_0$ is then also diagonal as intended. Each sign option of the condition $\mathbb{T}\sigma_x\mathbb{T}^\dagger = \pm\sigma_z$, is solved by two linearly independent transformations which we denote $\mathbb{T}^\pm_1$ and $\mathbb{T}^\pm_2$ with the given superscript indicating the sign of σ_z in the condition. Explicitly, we obtain

$$\mathbb{T}^\pm_1 = \frac{1}{\sqrt{2}}(\sigma_x \pm \sigma_z), \quad \mathbb{T}^\pm_2 = \frac{1}{\sqrt{2}}(\mathbb{1} \pm i\sigma_y). \quad (28)$$

All transformations fulfill $\mathbb{T}^\dagger = \mathbb{T}^{-1} = \mathbb{T}$ and are of Bogolyubov-Valatin type but without momentum or frequency dependence.

Notably, trying to generalize the previous approach to $\varepsilon_d \neq -U/2$ changes the matrix structure of $(\mathbb{G}^D_0)^{-1}$ considerably by adding an extra diagonal term proportional to $(\varepsilon_d + U/2)\sigma_z$. Diagonalizing $(\mathbb{G}^D_0)^{-1}$ by $\mathbb{T}$ would now require to simultaneously fulfill not only $\mathbb{T}\sigma_x\mathbb{T}^\dagger = \pm\sigma_z$ but also $\mathbb{T}\sigma_z\mathbb{T}^\dagger = \pm\sigma_z$ or $\mathbb{T}\sigma_z\mathbb{T}^\dagger = \pm\mathbb{1}$. Neither of the two combined conditions is, however, solvable. Consequently, outside of the half-filled case there exists no unitary transformation to diagonalize $(\mathbb{G}^D_0)^{-1}$. For example, applying $\mathbb{T}$ in the form of Eq. (28) away from the half-filling rotates the superconducting terms onto the diagonal elements of $(\mathbb{G}^W_0)^{-1}$ which is, however, traded off for rotating the originally diagonal terms proportional to $(\varepsilon_d + U/2)\sigma_z$ into off-diagonal terms proportional to $(\varepsilon_d + U/2)\sigma_x$. From now on, we therefore concentrate *exclusively on the half-filled case*.

Although, for the noninteracting ($U = 0$) half-filled case the corresponding Green function can be diagonalized by transformations (28), in the end, in the full interacting case the action of transformations (28) on the interaction part H_U needs to be considered. As shown in the Appendix A, using

the interaction term mixed of quadratic and quartic terms according to Eq. (13) allows us to obtain the Hubbard interaction term when the transformation $\mathbb{T}_1^-$ is used. Explicitly:

$$H_U = U w_\uparrow^\dagger w_\uparrow w_\downarrow^\dagger w_\downarrow. \qquad (29)$$

The remaining options for $\mathbb{T}$ produce all an extra quadratic term in H_U which is proportional to σ_x, thus spoiling the diagonal form of $\mathbb{G}_0^W(\omega^+)$. We thus select the transformation $\mathbb{T}_1^-$ in what follows and denote it as $\mathbb{T} \equiv \mathbb{T}_1^-$. Nevertheless, we stress that the remaining choices would also be possible when different partitionings of the full Hamiltonian are considered. Moreover, the transformation $\mathbb{T}_2^+$ fully corresponds to the transformation used in the standard NRG treatments of magnetic impurities coupled to superconducting reservoirs (see Refs. [35,36] for more detail) while $\mathbb{T}_1^+$ relates to the transformations applied in the Refs. [37–39] to solve the $\Delta \to \infty$ limit of the present model. However, in all of the aforementioned references, even at the half-filling the lead transformations corresponding to $\tilde{\mathbb{T}}_\alpha$ are explicitly performed within the applied NRG algorithms.

Since the resulting $\mathbb{G}_0^W(\omega^+)$ is proportional to $\omega\sigma_z g_1(\omega) + g_2(\omega)\mathbb{1}$ with $g_1(\omega)$ and $g_2(\omega)$ being even functions of ω we may actually drop the matrix Nambu formalism and employ directly the $w_\uparrow^\dagger$ and $w_\downarrow^\dagger$ fields which constitute the W spinor. We stress out in this regard, that such a transition requires us to change the hole propagator $\mathbb{G}_0^W(\omega^+)$ to an electron propagator which involves simultaneous change of the frequency sign as well as one extra minus sign for normal ordering of the creation and annihilation operators to obtain the corresponding spin-down electron propagator of the constituent field $w_\downarrow^\dagger$. In detail, $\omega g_1(\omega)\sigma_z \to \omega g_1(\omega)\mathbb{1}$ and $g_2(\omega)\mathbb{1} \to g_2(\omega)\mathbb{1}$. Thus, one obtains

$$G_{0\uparrow}^W(\omega^+) = G_{0\downarrow}^W(\omega^+) = \frac{1}{\omega + U/2 - \Sigma^W(\omega^+)} \qquad (30)$$

and the independence of Green functions of the spin index of the field w becomes explicit. The calculation of $\Sigma^W(\omega^+) = \Sigma_n^D(\omega^+) - \Sigma_a^D(\omega^+)$ can be performed for arbitrary bandwidth as shown in the Appendix B. In the limit of infinitely wide band $B \to \infty$, it takes the following form:

$$\Sigma^W(\omega^+) = -i\Gamma_N - \Gamma_S \left[\frac{i\,\mathrm{sgn}(\omega)}{\sqrt{\omega^2 - \Delta^2}}\Theta(\omega^2 - \Delta^2) \right.$$
$$\left. + \frac{\Theta(\Delta^2 - \omega^2)}{\sqrt{\Delta^2 - \omega^2}} \right]\left(\omega - \Delta\cos\frac{\varphi}{2}\right), \qquad (31)$$

where Θ is the Heaviside step function. The imaginary part of Eq. (31) is traditionally referred to as the hybridization function, see also Sec. IV A, while the real part is connected to the imaginary one via the Kramers-Kronig relations.

Taking together, the unitary transformation $\mathbb{T}$ allows us to map the original nondiagonal model expressed via D spinor onto a model described in terms of Bogolyubov-type quasiparticles w_σ coupled to a single normal lead which has an altered TDOS due to the frequency-dependent self-energy $\Sigma^W(\omega^+)$. Moreover, the Bogolyubov quasiparticles w_σ interact locally via the ordinary Hubbard interaction term. This allows us to redefine the three-terminal setup as one-channel-lead problem similar to the ordinary SIAM and apply NRG in a straight-

forward way as described in Ref. [43]. This way, all spectral properties in the spinor basis W can be obtained.

In the Nambu formalism of spinors D spin symmetry is manifestly present and the corresponding Nambu Green function has thus a normal component $G_n^D(\omega^+)$ and an anomalous $G_a^D(\omega^+)$. Because of Eqs. (29) and (30), spin symmetry is also preserved in the w basis and the resulting Green functions are thus spin independent, i.e. $G_\uparrow^W(\omega^+) = G_\downarrow^W(\omega^+) \equiv G_n^W(\omega^+)$. Even-though they can be directly calculated by means of NRG, in the end, we need to transform back to the original basis of the d electrons. Therefore, one needs to relate the Green functions and their corresponding spectral functions between both bases. Since the unitary transformation $\mathbb{T}$ mixes the original d_σ and $d_\sigma^\dagger$ fields only in a linear way, we obtain

$$G_n^D(\omega^+) = \tfrac{1}{2}\left[G_n^W(\omega^+) - G_n^W(-\omega^+)\right], \qquad (32)$$

$$G_a^D(\omega^+) = -\tfrac{1}{2}\left[G_n^W(\omega^+) + G_n^W(-\omega^+)\right], \qquad (33)$$

where $-\omega^+ = -\omega - i\eta$. Recall that $G_n^W(\omega^+) = G_n^{W*}(\omega^-)$ with $\omega^- \equiv \omega - i\eta$ and the imaginary part of the Green function equals the spectral function up to a multiplicative factor $-1/\pi$. Therefore, we can directly construct the normal spectral function $A_n^D(\omega)$ and the anomalous spectral function $A_a^D(\omega)$ in the d basis using

$$A_n^D(\omega) = \tfrac{1}{2}\left[A_n^W(\omega) + A_n^W(-\omega)\right], \qquad (34)$$

$$A_a^D(\omega) = -\tfrac{1}{2}\left[A_n^W(\omega) - A_n^W(-\omega)\right], \qquad (35)$$

with A_n^W being the spectral function corresponding to G_n^W. We will often refer to the backwards transformations of the normal spectral and anomalous function as symmetrization and antisymmetrization, respectively.

III. $\Delta \to \infty$ CASE

To demonstrate and assess the concepts derived in Sec. II, we turn first to the well-understood $\Delta \to \infty$ case of the present model and compare it to the standard NRG approach used to solve this limit in Refs. [34,37–39]. Here, one first applies a $\mathbb{T}$-like transformation to the dot electrons and a combination of $\mathbb{T}$-like and particle-hole transformations to the remaining Wilson chain. As unnoticed by the authors of Refs. [37–39], in the particle-hole symmetric case only the $\mathbb{T}$ transformation to the dot electrons is essential and the rest is just method specific. To show this, we briefly review the approach in Refs. [37–39]. Crucially, the $\Delta \to \infty$ Hamiltonian simplifies down to

$$H_{\Delta \to \infty} = H_{d,0} + H_U + H_N + H_{T,N} - \Delta_d(\varphi)(d_\uparrow^\dagger d_\downarrow^\dagger + d_\downarrow d_\uparrow), \qquad (36)$$

where $\Delta_d(\varphi) \equiv \Gamma_S\cos(\varphi/2)$, H_N, $H_{d,0}$, $H_{T,N}$ follow our previous notations and ε_d was considered originally as arbitrary. $H_{\Delta \to \infty}$ has thus a one-channel-lead form. The BCS effects are present via nonzero off-diagonal terms.

To treat those, the logarithmically discretized version of $\Delta \to \infty$ model is mapped onto a semi-infinite Wilson hopping chain with the first node populated by the local d_σ electrons ($\sigma \in \{\uparrow, \downarrow\}$) of the QD while remaining sites labeled by $i \in N$ are populated by fermions $c_{i\sigma}$ representing the bath

degrees of freedom. In Refs. [37–39], each site of the Wilson chain is rotated using unitary transformation O_Θ

$$O_\Theta = \begin{pmatrix} \cos\frac{\Theta}{2} & -\sin\frac{\Theta}{2} \\ \sin\frac{\Theta}{2} & \cos\frac{\Theta}{2} \end{pmatrix}, \quad (37)$$

which acts on the Nambu spinors of the given site of the Wilson chain, while

$$\cos\frac{\Theta}{2} = \sqrt{\frac{1}{2} + \frac{\tilde{\varepsilon}_d}{2\delta}}, \quad \sin\frac{\Theta}{2} = \sqrt{\frac{1}{2} - \frac{\tilde{\varepsilon}_d}{2\delta}}, \quad (38)$$

with $\delta = \sqrt{\tilde{\varepsilon}_d^2 + \Delta_d^2}$ and $\tilde{\varepsilon}_d = \varepsilon_d + U/2$. The first site of the Wilson chain transforms for example as

$$O_\Theta D = O_\Theta \begin{pmatrix} d_\uparrow \\ d_\downarrow^\dagger \end{pmatrix} = \begin{pmatrix} w_\uparrow \\ w_\downarrow^\dagger \end{pmatrix} \equiv W, \quad (39)$$

where D, W follow the notation of Sec. II. The sites representing the lead electrons (index i) are also subjected to particle-hole transformations. The coefficients of the resulting diagonal semi-infinite Wilson chain are then noticed to be identical with those of the ordinary asymmetric SIAM and because of the Hausholder transformation the equivalence of the $\Delta \to \infty$ model to the asymmetric SIAM with the particle-hole asymmetry factor δ from (38) and constant TDOS is established [37–39]. We stress that the findings in Refs. [37–39] hold at arbitrary filling.

Using the approach of Sec. II we may now prove that in the half-filling, only the unitary transformation O_Θ applied to the space of local electrons is essential while all of the remaining transformations are merely an NRG related technical tool. First, in the half-filled case $\tilde{\varepsilon}_d = \varepsilon_d + U/2 = 0$ corresponding to $\Theta = \pi/2$ for which the O_Θ transformation becomes $\mathbb{1}_2^+$ of Sec. II while the self-energy contribution of the leads is known to be proportional to the 2×2 unit matrix in the d basis of the local electrons. Thus, it is form invariant under any unitary transformation with $\Sigma_N^D(\omega) = \Sigma_N^W(\omega)$. The off-diagonal parts of the Hamiltonian (36) turn out to be more delicate. Performing then the same partitioning of (36) as in Eqs. (11) and (13), we may apply the transformation $O_{\pi/2}$ to obtain the noninteracting part of the dot Hamiltonian in a diagonal form

$$H_{d,0} = W^\dagger \begin{pmatrix} \delta - \frac{U}{2} & 0 \\ 0 & -\delta + \frac{U}{2} \end{pmatrix} W. \quad (40)$$

Applying then the transformation $O_{\pi/2}$ to the interaction term gives back (29) which finally proofs that the $\Delta \to \infty$ model maps onto the asymmetric SIAM with constant TDOS with the particle-hole asymmetry parameter $\delta = \Gamma_S \cos(\varphi/2)$. The resulting Wilson chain is identical to that of Refs. [37–39]. The physical interpretations of the hybrid reservoir behavior are then easily accessible via the well-known results on asymmetric SIAM. Qualitatively, starting from the spectral function $A_n^W(\omega)$ of the asymmetric SIAM of given asymmetry parameter $\delta = \Gamma_S \cos(\varphi/2)$ one applies the symmetrization procedure (34) and obtains the normal spectral function $A_n^D(\omega)$ of the three-terminal $\Delta \to \infty$ model in the original basis of the d fields. For the anomalous functions (subscript a), analogically, the antisymmetrization (35) is performed as shown Fig. 2.

In the top row of panels we show the spectral functions of the asymmetric SIAM in descending order of δ [49]. The middle row of panels shows then the symmetrized counterparts of the top row panels which actually represent the solution to the normal spectral functions of the $\Delta \to \infty$ model at given φ. Analogically, the bottom row shows the antisymmetrization of the top-row panels which then represent the anomalous spectral functions of the $\Delta \to \infty$ model. Panels in the same columns thus correspond to each other via the relation $\delta = \Gamma_S \cos(\varphi/2)$ and are ordered from left to right with the increasing phase difference φ for the $\Delta \to \infty$ model and in decreasing order of the asymmetry parameter δ of the underlying SIAM. The particle-hole symmetric case of the effective SIAM is then realized at $\varphi = \pi$.

Thus, in the w basis, the particle-hole symmetry at $\varphi = \pi$ leads to the appearance of an ordinary Kondo resonance of $A_n^W(\omega)$ at the Fermi energy. Additionally, two satellite Hubbard peaks emerge at approximately $\pm U/2$ (see the last column of panels in Fig. 2). Symmetrization (34) does not alter the shape of the normal spectral function which remains the same in both bases.

Decreasing the phase difference φ and keeping parameters U, Δ, Γ_N, and Γ_S constant drives the underlying asymmetric SIAM away from its particle-hole symmetric point as shown in the top row of panels of Fig. 2 (δ increases from right to left). As δ increases, the central Kondo peak shifts gradually away form the Fermi energy and becomes simultaneously broader and slightly smaller [50]. When the particle-hole asymmetry in the w basis is relatively small, i.e., $\delta = 2.5$ in Fig. 2, the off-central movement does not overcome its broadening. Consequently, performing symmetrization operation (34) to obtain $A_n^D(\omega)$ makes the central peak broader but still singly peaked. However, decreasing the angle φ further eventually causes such a strong decentralization that the broadening is insufficient. Symmetrization (34) then only leads to a split central peak with the remnants of Kondo resonances, as seen at larger φ corresponding to $\delta = 4.33$ and $\delta = 5.0$ cases in Fig. 2. At such a critical value, $\varphi^* \approx \pi/3$ in Fig. 2, the splitting of $A_n^D(\omega)$ is related to sufficient suppression of the Kondo correlations in the w basis. However, keeping the value of Γ_S so small that for given interaction strength U the asymmetry parameter δ is insufficient to destroy Kondo correlations, splitting might be avoided in analogy to SCIAM.

At $\varphi = 0$ (the first column of Fig. 4), the split-peak is accompanied by a highly suppressed pair of peaks at $\omega \approx \pm 12\Gamma_N$ which intensifies and shifts toward the Fermi energy as the angle φ is increased because the corresponding charge excitations of the underlying asymmetric SIAM become stronger (δ decreases). Therefore, at $\varphi^* \approx \pi/3$, when the split-peak merges into a Kondo-like central peak, this pair becomes well visible. Moreover, a second pair starts to emerge from the Kondo-like peak (note the shoulders of the central peak at $\varphi = 2\pi/3$ in Fig. 2). These two pairs move then toward $\pm U/2$ until they merge at $\varphi = \pi$ where they correspond to the ordinary Hubbard peaks of the symmetric SIAM. The behavior of the off-center peaks thus highly resembles that of the ABS states in the SCIAM (apart of the existence of two pairs also for $\varphi < \varphi^*$).
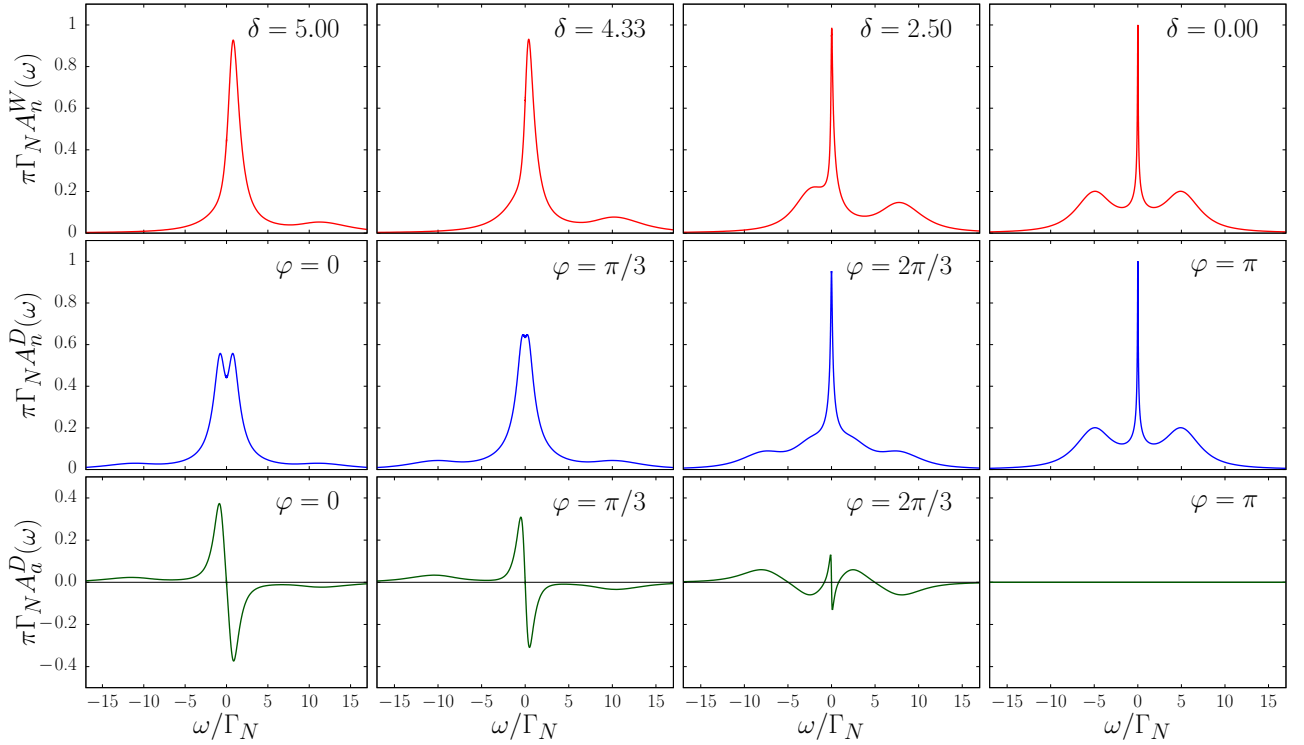
FIG. 2. The top row of panels shows the normal spectral functions for the asymmetric SIAM with $U = 5\Gamma_N$ in the direction of decreasing asymmetry parameter δ. The top row spectral functions also correspond to the spectral functions $A_n^W(\omega)$ of the $\Delta \to \infty$ model expressed in the w basis when U and Γ_N are the same and $\delta = \Gamma_s \cos(\varphi/2)$. The middle row of panels shows the normal spectral functions $A_n^D(\omega)$ of the $\Delta \to \infty$ model in the d basis obtained by symmetrization (34) of $A_n^W(\omega)$ corresponding to the top row. The bottom row shows the anomalous spectral function $A_a^D(\omega)$ of the $\Delta \to \infty$ model in the d basis obtained by antisymmetrization (35) of the top row.

The normal lead of the $\Delta \to \infty$ model causes not only a singlet ground state for all values of φ but also lifts the strict selection rules present in SCIAM which explains the additional pair of peaks for $\varphi < \varphi^*$. Thus, for $\varphi < \varphi^*$ the spectral function $A_n^D(\omega)$ resembles somewhat broadened spectral function of the 0 phase of SCIAM and is thus referred

to as 0-like phase in what follows. For $\varphi > \varphi^*$, $A_n^D(\omega)$ obtains a shape similar to that of broadened spectral function in the π phase of SCIAM. However, due to the normal electrode a Kondo resonance coexists with four broadened ABS states.
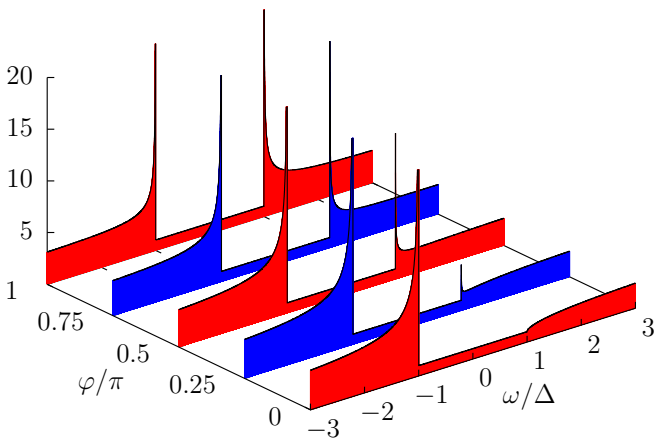

FIG. 3. Phase evolution of the TDOS $\Gamma^W(\omega)$ (41) in the w basis for $\Gamma_N = \Delta$ and $\Gamma_s = 2\Delta$. At $\varphi = 0$, only the left BCS singularity does appear and the resulting TDOS is highly asymmetric. Increasing φ diminishes the asymmetry while BCS singularities develop at both gap edges. The symmetry is fully restored only at $\varphi = \pi$.
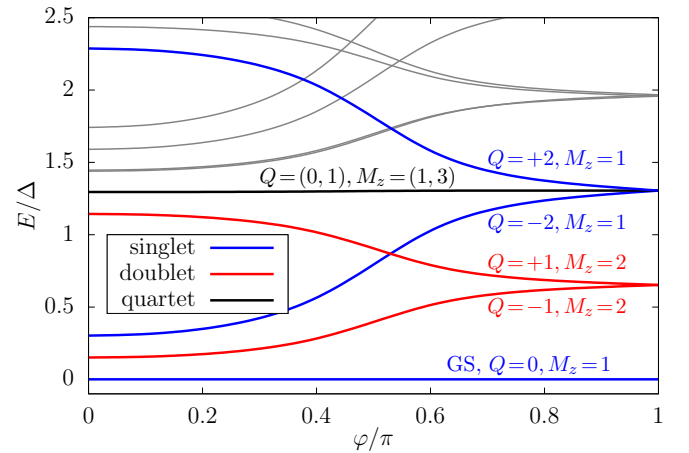

FIG. 4. Low-energy eigenvalues of the logarithmically discretized Hamiltonian obtained using NRG Ljubljana for the half-bandwidth $B = 2000\Delta$, $U = 3\Delta$, $\Gamma_S = \Delta$, and $\Gamma_N = \Delta/100$. Q is defined as the total charge of the Wilson chain measured with respect to the half-filling and $M_z \equiv 1 + 2S_z$ with S_z being the overall magnetization of the Wilson chain.

IV. FINITE-GAP MODEL

A. NRG calculations

As shown in Sec. II C, the transformation $\mathbb{T}$ maps the finite-gap three-terminal setup at the half-filling onto an NRG-tractable one-channel problem. In the w basis, the Hamiltonian describes an Anderson impurity coupled to a continuum of bath states with modified TDOS $\Gamma^W(\omega)$ corresponding to $\Sigma^W(\omega)$ which except of $\varphi = \pi$ is particle-hole asymmetric as shown in Appendix B. In the limit of infinitely wide band it reads

$$\Gamma^W(\omega) = \Gamma_N + \frac{\Gamma_S|\omega|\Theta(\omega^2 - \Delta^2)}{\sqrt{\omega^2 - \Delta^2}}\left(1 - \frac{\Delta}{\omega}\cos\frac{\varphi}{2}\right), \quad (41)$$

where Θ is the Heaviside step function. The phase evolution of hybridization function $\Gamma^W(\omega)$ is shown in Fig. 3 for selected parameters. Note, that $\Gamma^W(\omega)$ is only particle-hole symmetric at $\varphi = \pi$ with asymmetry increasing toward $\varphi = 0$ in analogy to the $\Delta \to \infty$ case. Since $\Gamma^W(\omega)$ is diagonal, in the w basis standard one-channel NRG method of Refs. [40,43] can be applied. To this end, we have utilized NRG Ljubljana code [45] with intertwined z discretization according to the scheme of Žitko *et al.* [51], i.e., $z = n/10$ where $n \in \{0, \dots, 10\}$. To achieve smoother spectral functions with discontinuities at the BCS gap edges, the so-called self-energy trick has been employed. We stress that in the main body of the article we concentrate on the wide band limit with bandwidth set to $2B = 4000\Delta$. The corrections for the case of a narrow band are discussed in the Appendix B.

The experimentally accessible spectral functions in the d basis have been obtained by means of Eqs. (34) and (35) and the results are discussed in Sec. IV B. On-dot induced pairing $\nu = \langle d_\downarrow d_\uparrow \rangle$ is trivially connected to the filling n_w in the w basis and can be measured directly as discussed in Sec. IV C. The operator for the Josephson current depends explicitly from the lead electrons and an integral formula of Ref. [52] involving the anomalous component of Green function in the d basis is required as discussed in Sec. IV C.

Most importantly, we note that the energy eigenvalues, as obtained at each NRG iteration, are basis independent because $\mathbb{T}$ is unitary. Corresponding effective models attributed to certain RG fixed point can thus be directly read off. Here, we concentrate exclusively at low temperature behavior which is governed by the strongly coupled (SC) or frozen impurity RG fixed point depending on the extent of phase-bias-induced particle-hole asymmetry in the w basis as shown in Fig. 4. Here, we selected parameters involving a sign reversal of the local pairing at $\varphi_{\text{pair}}^* \approx 0.45\pi$ and Josephson current reversal at $\varphi_j^* \approx 0.5\pi$ (see the discussion in Sec. IV C). At $\varphi = \pi$, the SC fixed point of ordinary symmetric SIAM is identified since it contains a singlet ground state, followed by first a quadruplet and then a sextet of next excited levels. Decreasing φ, splits the quadruplet into two doublets while the sextet splits into two singlets placed symmetrically around the remaining quadruplet corresponding to the behavior of ordinary asymmetric SIAM at small particle-hole asymmetry. This, establishes then a correspondence of the present three-terminal set-up to the particle-hole asymmetric SIAM at $\varphi \neq \pi$ with particle-hole symmetric case recovered at $\varphi = \pi$. The quali-

tative behavior of the spectral functions is therefore expected to essentially follow the results of the $\Delta \to \infty$ case discussed in Sec. III. The quantitative changes in on-dot induced pairing and Josephson current are therefore only related to the fine details of the corresponding spectral functions at higher frequencies as discussed in Secs. IV B and IV C.

B. Spectral properties and the Kondo scale

The phase evolution of the normal spectral function in the d basis shown in Fig. 5 for two values of U/Δ demonstrates that qualitatively finite-gap case does not differ much from the $\Delta \to \infty$ case. Selecting first the $U = 3\Delta$ case [Figs. 5(a) and 5(b)], we notice two broadened ABS-like peaks placed symmetrically around the Fermi energy at $\varphi = 0$. With increasing φ, both peaks move toward the Fermi energy and merge at a certain value φ^* which depends nontrivially on U and Δ. Subsequently, for all $\varphi > \varphi^*$ the central Kondo-like peak is present. Moreover, four side-peaks (corresponding to the two symmetrized effective Hubbard satellites in the w basis) also emerge. Increasing φ further shifts the two peaks on each side of the spectra together, until at $\varphi = \pi$ they coalesce. At this point, the TDOS is symmetric and the $\varphi = \pi$ spectrum resembles the typical three-peak structure of the symmetric SIAM. The second case with $U = 6\Delta$ is shown in Figs. 5(c) and 5(d). Here the ratio Γ_S/Δ is insufficient to generate particle-hole asymmetry leading to the emergence of the 0-like phase. Such regimes are analogous to the observations made for SCIAM at large ratios U/Δ.

To make the movement of the in-gap peaks explicitly manifest, we visualized the phase-dependent positions of their maxima via heatmaps in Figs. 5(b) and 5(d). We clearly observe in Fig. 5(b) their crossing at angle φ^*. When φ is further increased, the in-gap peaks move apart again. However, for all $\varphi > \varphi^*$ two additional in-gap states emerge. The two peaks for $\varphi < \varphi^*$ can then be related to the two ABS states of SCIAM in the 0 phase, while the four off-central peaks are in one-to-one correspondence with the four ABS states observed in the π phase of SCIAM. However, unlike in SCIAM the nonzero TDOS around the Fermi energy gives rise also to the central Kondo-like resonance for all $\varphi > \varphi^*$.

Thus, the obtained spectral functions qualitatively correspond to the $\Delta \to \infty$ model and the physical interpretation in terms of the particle-hole asymmetry of the underlying model in the w basis holds analogously. Nevertheless, there are quantitative differences which appear once integral quantities, such as the filling n_w in the w basis, are considered. For the $\Delta \to \infty$ model, the filling n_w monotonically decreases from the $n_w = 1$ value obtained at $\varphi = \pi$ for all parameter regimes. In the finite-gap three-terminal case, there are parameter regimes where n_w first increases to values larger than 1 (positive effective chemical potential) and then starts to monotonically decrease to values smaller than 1 (negative effective chemical potential). Such integral properties are shown in Sec. IV C to be crucial for the system to exhibit effects such as pairing or Josephson current reversal which are typical of 0-π transition observed in SCIAM. This means that the precise shape of spectral functions plays an important role when analyzing the finite-gap case.

In Sec. IV A, we have already established the correspondence of the low-energy many-body NRG spectra to that of
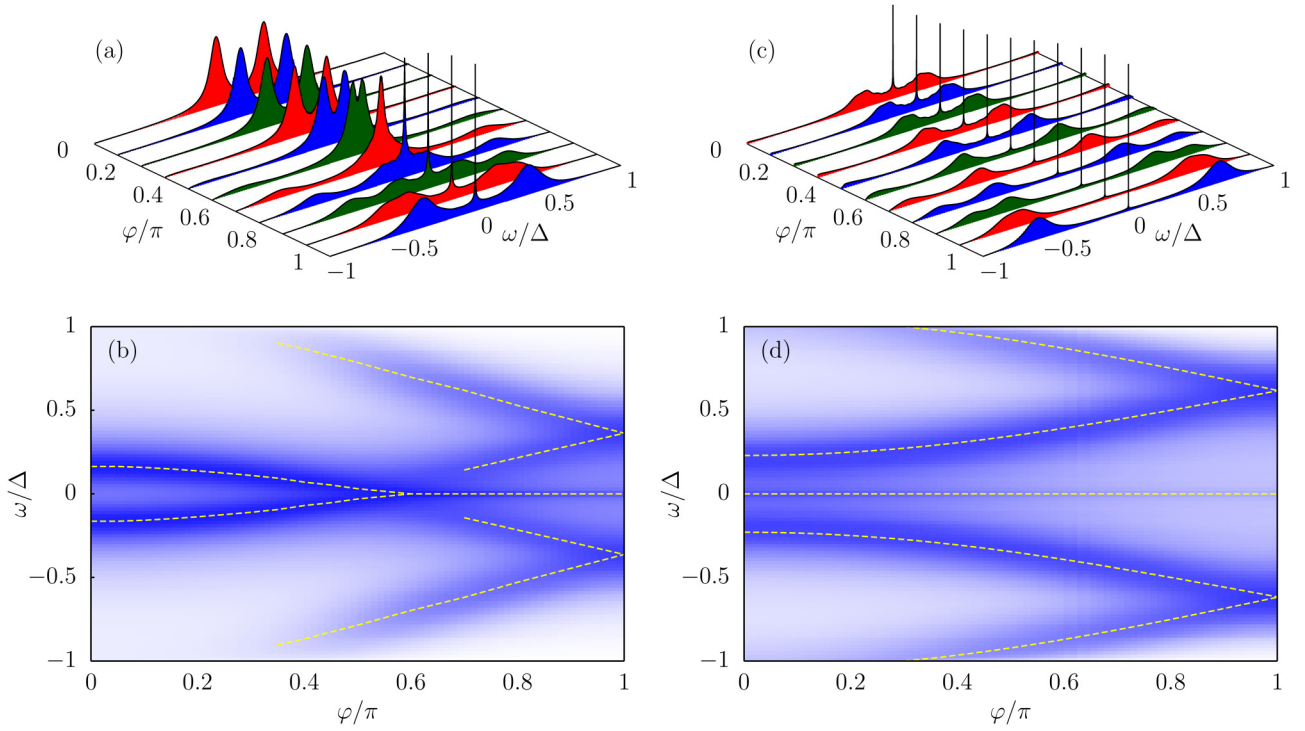
FIG. 5. (a) Phase evolution of the spectral function $A_n^D(\omega)$ in the subgap region of the finite-gap three-terminal setup for $U = 3\Delta$, $\Gamma_N = \Delta/10$, $\Gamma_S = \Delta$ and half-bandwidth $B = 2000\Delta$. For $\varphi < \varphi^* \approx 0.55\pi$ one observes a pair of broadened ABS states while for $\varphi > \varphi^*$ an additional pair of broadened ABS states and an additional central Kondo-like peak do appear. In analogy to the SCIAM, for $\varphi < \varphi^*$ the regime is referred to as the 0-like phase while for $\varphi > \varphi^*$ as the π-like phase. (b) Heatmap corresponding to panel (a) highlights the phase-dependent position of the maxima of the in-gap peaks (dashed lines). (c) The same as in panel (a) only $U = 6\Delta$. The Kondo correlations dominate the system which remains in the π-like phase for all values of φ. For sufficiently large U, such a scenario does occur also in the SCIAM. (d) Heatmap corresponding to panel (c) shows the phase-dependent position of the maxima of the in-gap peaks (dashed lines).

the particle-hole asymmetric SIAM for $\varphi \neq \pi$ with particle-hole asymmetry monotonically decreasing toward $\varphi = \pi$ where it completely vanishes. In the w basis, one therefore observes that starting at the particle-hole symmetric case for $\varphi = \pi$ and then decreasing φ, causes a gradual movement of the original Kondo peak away from the Fermi energy which is induced by the increasing particle-hole asymmetry. However, as long as $\varphi > \varphi^*$ the increasingly large broadening does overcome this shift and symmetrization (34) still leads to a well-defined central peak in the spectral function $A_n^W(\omega)$. Only when φ is decreased further, does the broadening of the central peak stop compensating for the rapid movement of the peak, so that the symmetrization (34) results in a doubly peaked spectral function $A_n^W(\omega)$ in the w basis.

The lack or presence of a single central peak can thus be understood as a sign of the Kondo-like interaction-screening efficiency. To quantify such behavior, we have extracted the phase-dependent Kondo temperature T_K as the half-width at half maximum (HWHM) value of the zero-energy peak of the π-like phase. Unlike in Ref. [34], we first compare T_K to the Kondo temperature at $\varphi = \pi$, denoted as T_K^π, which as shown by the transformation $\mathbb{T}$ preserve particle-hole symmetry in the w basis. Decreasing φ from its particle-hole symmetric point at $\varphi = \pi$ then introduces increasingly larger particle hole asymmetry in the w basis and is also accompanied by the enhancement of T_K in the experimentally relevant d basis. Such a phase-dependent enhancement of T_K

is then conveniently measured via $\log(T_K/T_K^\pi)$ as done in Fig. 6.

The broadening of the central peak in the experimentally observed d basis, as encoded by T_K, is thus accomplished by a delicate interplay between the shift and broadening of the central peak in the w basis due to the increase of the particle-hole asymmetry. Once the symmetrization (34) is applied, the two effects combine to a wide and somewhat deformed central peak in the d basis as compared to the particle-hole symmetric case $\varphi = \pi$. The increasing T_K therefore cannot be completely attributed to the increase of Kondo correlations, as speculated in Ref. [34], as charge fluctuations become more important and may even lead to complete destruction of the central Kondo peak once the crossover to the 0-like phase is entered. Consequently, the enhancement of T_K with decreasing φ is to be attributed to the increase of the underlying particle-hole asymmetry of the system as seen in the w basis introduced in Sec. II.

Predictions on the phase-dependent enhancement according to $\log T_K \propto \cos^2(\varphi/2)$ were performed already in Ref. [34] but were based only on numerical indications from the second order perturbation theory. To thoroughly assess this conjecture we thus use the exact NRG data for $\Gamma_N = \Delta/10$ at various U, see the upper panel of Fig. 6. The phase-dependent spectral functions corresponding to $U = 3\Delta$ and $U = 6\Delta$ cases have already been presented in Fig. 5 from which it is evident that the region of π-like phase is considerably
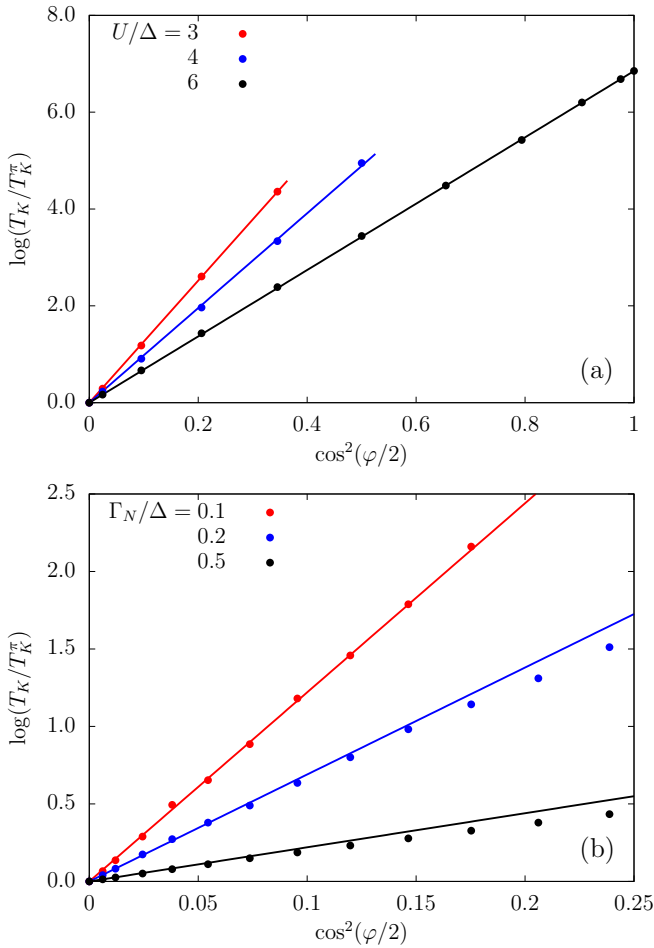
FIG. 6. (a) Phase dependence of the Kondo temperature T_K of the three-terminal set-up at $\Gamma_S = \Delta$, $\Gamma_N = \Delta/10$ at varying U with half-bandwidth $B = 2000\Delta$. T_K is determined as HWHM of the central Kondo-like peak observed in the π-like phase, T_K^π denotes T_K at $\varphi = \pi$. Points represent NRG data while lines are fits in the corresponding π-like phase regions. In all three cases, $\log T_K \propto \cos^2(\varphi/2)$ and follows the hypothesis of Ref. [34]. (b) The same as in panel (a) at fixed $U = 3\Delta$ and varying Γ_N. The solid lines now represent tangents at $\cos(\varphi/2) = 0$ ($\varphi = \pi$). For higher values of Γ_N the $0 - \pi$-like crossover region is only insignificantly shifted toward lower values of φ [higher values of $\cos(\varphi/2)$]. The range of the horizontal axis is thus selected to be narrower compared to panel (a), i.e., $0 \leqslant \cos^2(\varphi/2) \leqslant 1/4$ ($2\pi/3 \leqslant \varphi \leqslant \pi$). Exceeding $\Gamma_N = \Delta/5$ we observe clear deviations from the hypothesis of Ref. [34] which are due to the BCS electrons directly entering the formation of the Kondo resonance.

increasing with U at fixed Γ_N. Since the HWHM as a measure of T_K becomes meaningless below a given φ^*, the corresponding dependencies in the upper panel of Fig. 6 terminate at their corresponding φ^* and only the case $U = 6\Delta$ covers the whole available φ range. Nevertheless, in all three cases we observe that $\log T_K$ is proportional to $\cos^2(\varphi/2)$ with no significant deviations appearing when approaching the crossover region around φ^*. In these parameter regimes, the hypothesis of Ref. [34] is thus very well satisfied.

However, when Γ_N is increased up to the size comparable with Δ, we expect the divergent portion of $\Gamma^W(\omega)$ present at

the gap edges to become more involved in the formation of the Kondo resonance. This in turn potentially deforms the central peak and may cause deviations from the $\log T_K \propto \cos^2(\varphi/2)$ law observed previously. To investigate such regime, we selected the $U = 3\Delta$ case shown previously and increased Γ_N, see Fig. 6(b). Since, the size of the π-like phase region is almost independent of Γ_N, we may focus onto the narrower range of $2\pi/3 \lesssim \varphi < \pi$ [$0 < \cos^2(\varphi/2) \leqslant 1/4$]. For $\Gamma_N = \Delta/5$ and $\Gamma_N = \Delta/2$ the phase dependencies obtained by NRG (points in the graph) follow the tangents at $\varphi = \pi$ [solid lines in Fig. 6(b)] quite closely. However, they start to deviate increasingly in the crossover region as φ is decreased toward φ^*. The deviations from the hypothesized $T_K \propto \cos^2(\varphi/2)$ law are, however, unrelated to entering the crossover region of the π-like to 0-like transition as follows from the $\Gamma_N = \Delta/10$ case [red points in Fig. 6(b)].

Let us now connect the findings to the expected experimental outcome. In the literature, there are numerous statements referring the *enhancement* of the Kondo scale upon switching on the superconductivity in the three-terminal setup [34,53,54]. The issue is, however, which reference system is used for the comparison (how the switch-on of the superconductivity is achieved). One option is to *add* the superconducting lead(s) to the conventional Anderson/Kondo model of a QD with one normal lead as used, for example, in Ref. [53] for the case of one added superconducting lead in the $\Delta \to \infty$ model. The resulting enhancement of T_K due to the addition of the superconducting lead is indisputable, nevertheless, in experiments, it would require the possibility of a controlled tunnel coupling/decoupling of the superconducting lead. While it is in principle possible by electrostatic gating of the pinch-off of the tunneling connection, the conventional experimental practice works differently—the reference normal system would not consist of the single normal lead but of all involved leads, including the superconducting one(s), turned into the normal state by a small magnetic field.

To quantify this matters, we first evaluate T_K of the three-terminal set-up with $\Gamma_S = 10$, $\Gamma_N = \Delta = B/2000$ ($2B$ being the bandwidth) at various interaction strengths U and for all phase differences compatible with π-like phase. The resulting values of T_K lie all in the blue shaded region of Fig. 7 with $\varphi = \pi$ cases being represented by the blue line in Fig. 7). First, we consider referencing the outcome against the case of both BCS electrodes completely decoupled from the present three-terminal set-up. Since $\Gamma_S = 0$, we note that the system is just the ordinary particle-hole symmetric SIAM with constant TDOS given by Γ_N. We thus denote the corresponding Kondo temperature as T_K^N and vary the interaction strength U at constant Γ_N (black line in Fig. 7). Clearly, $T_K > T_K^N$ for all values of U in the plotted region and further by extrapolation. Consequently, enhancement of the Kondo screening due to the additional BCS correlations is verified in accord with Refs. [34,53]. The second, experimentally more accessible option is obtained by setting $\Delta = 0$ (the phase dependence vanishes). The corresponding Kondo temperature is denoted then $T_K^{\Delta=0}$ (red line in Fig. 7). Now $T_K < T_K^{\Delta=0}$ for all plotted values of U and further by extrapolation. The introduction of the superconducting correlations is thus clearly *decreasing* T_K, which is also our prediction for the conventional experimental setups.
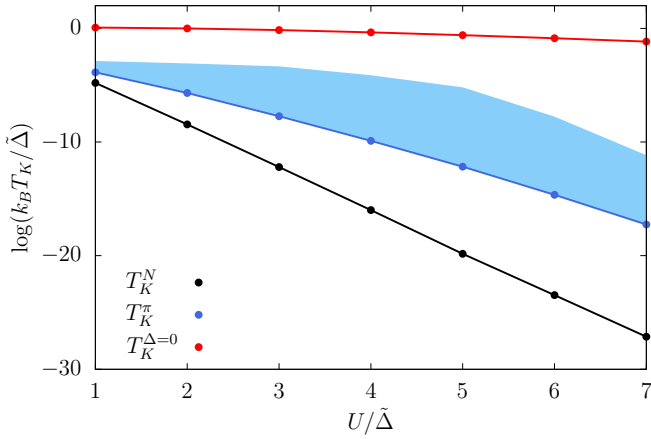
FIG. 7. Dependence of the Kondo temperature T_K on U for the three-terminal set-up (blue) and analogous systems with decoupled BCS leads (black) and with a closed BCS gap (red). T_K in all systems is defined via HWHM as in Fig. 6. Points represent NRG data while lines are just for visual guidance. We use $\tilde{\Delta} = B/2000$ as the unit of energy. The full three-terminal set-up (blue) is calculated at parameters $\Delta = \tilde{\Delta}$, $\Gamma_S = \tilde{\Delta}$, and $\Gamma_N = \tilde{\Delta}/10$. Blue points and the blue solid line represent values at $\varphi = \pi$ while the blue shaded region covers all φ values in π-like phase. Values for the decoupled BCS leads are obtained by setting $\Gamma_S = 0$ and keeping $\Gamma_N = \tilde{\Delta}/10$ in the full three-terminal set-up. The case of the closed gap is obtained by setting $\Delta = 0$ in the full three-terminal set-up and keeping the remaining parameters the same. It corresponds to the ordinary SIAM with the combined hybridization strength of all three metallic leads $\Gamma_N + \Gamma_S = 1.1\tilde{\Delta}$. Clearly, the Kondo temperature of the full three-terminal set-up is bounded between the other two cases.

C. Pairing and Josephson current

We now briefly address the transport properties in the hybrid three-terminal structure. Because they have already been obtained for finite temperatures in Ref. [34] using QMC, we will mostly concentrate on the methodology in our present approach and use the available results as a comparison to the $T = 0$ results presented here.

Although, the transformation $\mathbb{T}$ allows simpler Hamiltonian formulation of the present problem in the w basis, all transport properties are naturally measured in the original d basis. Superconducting effects are then related to the off-diagonal terms of the Hamiltonian, or equivalently to the off-diagonal Nambu Green functions, expressed in the d basis. Thus, for example, although the on-dot induced pairing in the w basis is by definition zero as $G^W(\omega)$ has no off-diagonal entries, one may show by simple application of the transformation $\mathbb{T}$ to the definition of ν that

$$\nu \equiv \langle d_\downarrow d_\uparrow \rangle = \frac{1}{2} - \frac{n_w}{2}, \qquad (42)$$

where $n_w \equiv n_{w\uparrow} + n_{w\downarrow}$ is the sum of occupations of the spin-up and spin-down levels in the w basis with $n_w = 1$ in half-filling. Interestingly, changing $n_w < 1$ to $n_w > 1$ in the above equation induces then sign reversal of ν.

Consequently, for $\Delta \to \infty$ model the mapping onto the ordinary asymmetric SIAM effectively prohibited any sign reversal of ν as $n_w < 1$ strictly. In the case of the finite-gap three-terminal setup, such restrictions are lifted and the

observed dependencies resemble closely the behavior of SCIAM (see Fig. 7). However, unlike in SCIAM no true phase transition is present and ν is a continuous function of φ with a crossover region of significant drop only visible for small Γ_N/Γ_S. For $\Gamma_N = \Gamma_S/100$ and $\Gamma_N = \Gamma_S/10$, ν even reverses sign at φ^*_{pair}. However, $\varphi^*_{\text{pair}} \neq \varphi^*$ as the two values coincide only for $\Gamma_N \to 0$. The comparison of the present results to QMC is shown in the the Appendix C, where also the effects of the finite bandwidth are discussed. At this place, it is sufficient to note that deep in the 0-like or π-like phase QMC and NRG agree well within their numerical accuracy.

To obtain the Josephson current J we note that the corresponding operator involves c electrons of the leads and we therefore use its expression in terms of the anomalous Green function $G_a^D(\omega^+)$ in the d basis [52]

$$J = 2 \tan\frac{\varphi}{2} \int_{-\infty}^{+\infty} \frac{d\omega}{\pi} f(\omega) \text{Im}\big[G_a^D(\omega^+) \Sigma_a^D(\omega^+) \big], \qquad (43)$$

where $f(\omega)$ is the Fermi-Dirac distribution, while the anomalous self-energy $\Sigma_a^D(\omega^+)$ reads in the limit of the infinite bandwidth

$$\Sigma_a^D(\omega^+) = \frac{\Gamma_S \Delta \cos(\varphi/2)}{\sqrt{\Delta^2 - \omega^2}} \Theta(\Delta^2 - \omega^2)$$
$$+ \frac{i\Gamma_S \Delta \cos(\varphi/2) \operatorname{sgn}(\omega)}{\sqrt{\omega^2 - \Delta^2}} \Theta(\omega^2 - \Delta^2). \quad (44)$$

The integral (43) involving anomalous components of the Green function requires high frequency resolution and reliable broadening procedure when applying NRG.

The results of phase-dependent Josephson current are shown in Fig. 8 for $U = 3\Delta$ at different ratios of Γ_N/Γ_S. The sign reversal of the Josephson current occurs only for small hybridization strengths Γ_N which clearly shows that Kondo correlations are important in the system and may overcome the superconducting correlations. Once again, the φ^*_j at which sign reversal occurs does not match φ^* from crossing of the ABS states nor φ^*_{pair}, but all three values tend to be the same for $\Gamma_N \to 0$.

V. CONCLUSIONS

We have investigated a general finite-gap model of QD with an arbitrary Coulomb repulsion attached to the hybrid reservoir composed of one normal lead and two BCS leads with an arbitrary phase difference. To obtain reliable and method-unbiased results on phase-dependent spectral functions, the standard NRG was employed. However, the full problem with three types of leads requires in the standard NRG approach the implementation of three-channel calculations which poses several nontrivial challenges [55]. To circumvent the numerical limitations we have thus introduced a unitary transformation $\mathbb{T}$ of the local dot electrons d, which despite the general belief [44] allows us to reformulate the present finite-gap three-terminal model as well as any general model with phase-biased superconductors involved, including SCIAM, as a one channel problem.

Since the present three-terminal reservoir has a nonzero TDOS around the Fermi energy a standard logarithmic discretization in the transformed basis of the fields w_σ with
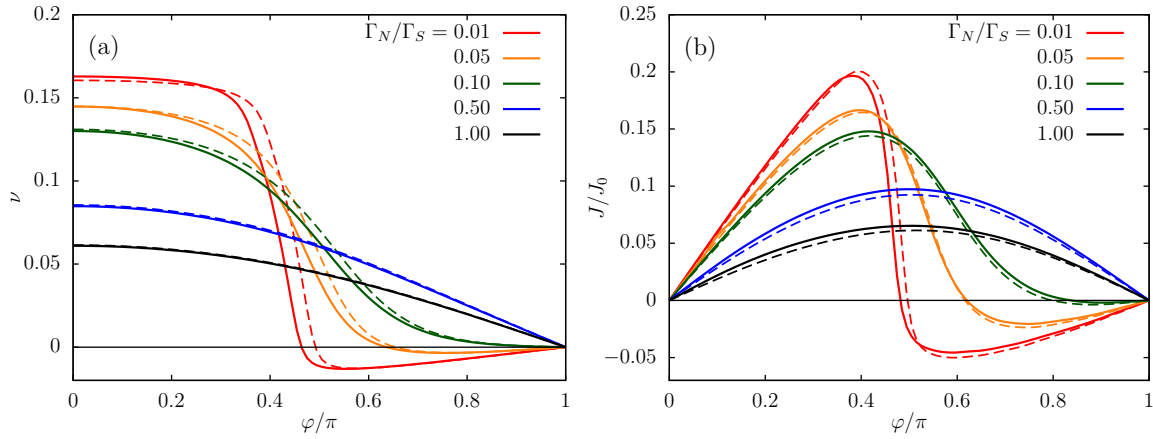
FIG. 8. (a) Phase evolution of the on-dot induced pairing $\nu \equiv \langle d_\downarrow d_\uparrow \rangle$ of the finite-gap three-terminal setup at $T = 0$ obtained using NRG Ljubljana in the w basis with subsequent use of Eq. (42) for the half-bandwidth $B = 2000\Delta$ (solid lines) and $B = 100\Delta$ (dashed lines). Parameters of the model are $U = 3\Delta$ and $\Gamma_S = \Delta$ while Γ_N varies. (b) Phase evolution of the Josephson current J with $J_0 = 2e\Delta/\hbar$ obtained using NRG Ljubljana in the w basis with subsequent use of Eq. (43) for the same parameters as in panel (a).

$\sigma \in \{\uparrow, \downarrow\}$ can be employed. Thus, the open-source NRG Ljubljana code could be employed unaltered. The obtained phase-dependent spectral functions showed behavior resembling that of the SCIAM, see also Figs. 5 and 8. Thus, two regimes, referred here as the 0-like and the π-like phase, have been identified in analogy. They do not however constitute separate phases since the nonzero TDOS around the Fermi energy leads to the formation of a singlet many-body ground state for any φ.

The width of the resulting crossover region, see Figs. 5 and 8, is roughly proportional to the hybridization Γ_N. Here, the off-center in-gap peaks of the corresponding spectral function do cross at φ^*, the on-dot induced pairing changes sign at φ^*_{pair} and the Josephson current at φ^*_j. Generally the values of φ^*, φ^*_{pair} and φ^*_j do not equal, but do so in the limit of $\Gamma_N \to 0$, where the corresponding SCIAM limit is obtained. However, in the limit of large Γ_N pairing and Josephson current are always positive and neither φ^*_{pair} nor φ^*_j are defined although φ^* still exists as the 0-like and the π-like distinct spectra are present.

Thus, for $\varphi > \varphi^*$, the presence of two pairs of the in-gap peaks which merge together at $\varphi = \pi$ and the presence of a central Kondo-like resonance defines the spectral property of the π-like phase. The two pairs of the in-gap peaks show an analogous phase-dependent behavior as the ABS states of the SCIAM as shown in Fig. 5 and they can consequently be understood as the broadened analogs of the ABS states of the SCIAM. However, the nonzero TDOS around the Fermi energy, as provided by the normal lead, allows screening of the spin of the QD even at $T = 0$ and leads to the formation of the Kondo peak in the spectral function of the π-like phase. Thus, unlike in the SCIAM, in the finite-gap three-terminal setup the broadened ABS states do coexist with the Kondo resonance in the π-like phase as shown in Figs. 5(a) and 5(c).

Nevertheless, at φ^* the central peak at the Fermi energy splits and can no longer be attributed to Kondo-like correlations since charge excitations dominate the effective underlying model which is strongly out of the half-filling. Thus, for $\varphi < \varphi^*$ the 0-like region is entered with the spectral weight at the Fermi energy moving toward zero with further

decreasing φ. The resulting split peak can then be interpreted in terms of two broadened ABS states of phase-dependent behavior resembling the SCIAM. However, such a 0-like phase has an additional pair of low-intensity peaks at higher frequencies, which (unlike in SCIAM) can be excited in the one-particle manner due to admixtures of the doublet state induced by the coupling to the normal lead.

Such a complex behavior is qualitatively explained via the transformation $\mathbb{T}$ which is thus not merely a technical tool for the NRG implementation. The TDOS in the w basis is highly particle-hole asymmetric at $\varphi = 0$. Then, with increasing φ, its asymmetry is continuously diminished until at $\varphi = \pi$ it completely vanishes. As shown in Fig. 4, the particle-hole asymmetry of the TDOS effectively acts as the particle-hole asymmetry in an ordinary SIAM with the concomitant increase of the Kondo temperature upon increasing the asymmetry followed by entering the mixed valence regime and eventually complete destruction of the Kondo resonance.

The Kondo temperature T_K can be quantitatively assessed via the phase-dependent HWHM of the central Kondo-like peak. The analysis in Sec. IV C (see also Fig. 6) showed that for $\Gamma_N \lesssim \Delta/10$ almost up to φ^*, the log T_K follows very well the $\cos^2(\varphi/2)$ trend hypothesized already in Ref. [34]. Thus, even though the hypothesis in Ref. [34] is based on the infinite-gap limit of the present model and the second-order perturbation theory, we have shown that it is robust and holds for sufficiently weak Γ_N. Significant deviations from the $\cos^2(\varphi/2)$ law start appearing roughly around $\Gamma_N \sim \Delta$.

Moreover, using the transformation $\mathbb{T}$ we have also obtained the phase-dependent on-dot induced pairing ν and the phase-dependent Josephson current J in various parametric ranges. Results in the limit of the infinitely wide band are presented in Fig. 8, where also effects of finite width of the band are shown (with a detailed derivation given in the Appendix B). Incorporating these corrections allowed for comparison with another numerically exact method, the continuous-time hybridization expansion (CT-HYB) QMC with a good agreement in the regions outside of the crossover while large temperature dependence smears the region itself, see Appendix C. The resulting pairing and supercurrent

reversals do not occur exactly at φ^* defined by the spectral functions and appear only at sufficiently low ratios Γ_N/Γ_S. Once a given threshold is exceeded and the Kondo screening dominates the system, superconducting correlations are essentially suppressed and only modify the phase-dependent transport. This behavior is enhanced by increasing the interaction strength, reducing the gap size, or increasing the hybridization of the normal lead. The observation of the 0-π-like crossover is thus possible only in a fairly small portion of the parameter space corresponding to the weak coupling of the normal lead to the QD.

The mapping $\mathbb{T}$ not only significantly reduces the numerical complexity of the hybrid normal-superconductor reservoirs, but it also allows for conceptual understanding of the competing Kondo and Josephson effects via the particle-hole asymmetric SIAM. In this regard, it is worth mentioning that the transformation $\mathbb{T}$ applies in the same form also to the SCIAM, i.e., an interacting QD coupled to two superconducting leads with hard gap in the spectrum, leading to its mapping onto the problem of normal Anderson impurity coupled to an insulator-like electronic reservoir with a hard spectral gap around the Fermi level. The original Nambu formulation becomes then a scalar one which may allow for new insights and is thus worth further pursuits. Moreover, as shown in Ref. [56, Fig. 3b], in the most interesting Kondo regime of the SCIAM model the results are in fact independent of the value of the particle-hole asymmetry for quite a wide range of its value. Therefore, even though the mapping $\mathbb{T}$ is restricted to the particle-hole symmetric model, the obtained results should be applicable also rather far away from this regime which makes the transformed scalar version of the SCIAM model practically relevant.

APPENDIX A: INTERACTION TERM IN THE w BASIS

The expression (29) is easily obtained by first applying the transformation $\mathbb{T}_1^-$ to the following quantities

$$d_\uparrow^\dagger d_\uparrow = \frac{1 + w_\uparrow^\dagger w_\uparrow - w_\downarrow^\dagger w_\downarrow}{2} - \frac{w_\uparrow^\dagger w_\downarrow^\dagger + w_\downarrow w_\uparrow}{2}, \quad (A1)$$

$$d_\downarrow^\dagger d_\downarrow = \frac{1 - w_\uparrow^\dagger w_\uparrow + w_\downarrow^\dagger w_\downarrow}{2} - \frac{w_\uparrow^\dagger w_\downarrow^\dagger + w_\downarrow w_\uparrow}{2}. \quad (A2)$$

Since $\mu = w_\uparrow^\dagger w_\uparrow - w_\downarrow^\dagger w_\downarrow$ and $\xi = w_\uparrow^\dagger w_\downarrow^\dagger + w_\downarrow w_\uparrow$ satisfy

$$1 - \mu^2 = \xi^2 = -w_\uparrow^\dagger w_\uparrow + 2n_{w\uparrow}n_{w\downarrow} + w_\downarrow w_\downarrow^\dagger, \quad (A3)$$

$$\mu\xi = \xi\mu = 0, \quad (A4)$$

with $n_{w\uparrow} = w_\uparrow^\dagger w_\uparrow$ and $n_{w\downarrow} = w_\downarrow^\dagger w_\downarrow$, we obtain

$$d_\uparrow^\dagger d_\uparrow d_\downarrow^\dagger d_\downarrow = \frac{1 - \mu^2 - \mu\xi + \xi\mu - 2\xi + \xi^2}{4}$$

$$= n_{w\uparrow}n_{w\downarrow} - \frac{1}{2}W^\dagger(\sigma_x + \sigma_z)W. \quad (A5)$$

Applying then $\mathbb{T}_1^-$ to the interaction term H_U gives

$$H_U = U d_\uparrow^\dagger d_\uparrow d_\downarrow^\dagger d_\downarrow - \frac{U}{2}D^\dagger(\sigma_x + \sigma_z)D = U w_\uparrow^\dagger w_\uparrow w_\downarrow^\dagger w_\downarrow, \quad (A6)$$

which in the w basis obtains the form of the ordinary Hubbard term. Notice that the additional quadratic term in H_U in the d basis cancels exactly the quadratic term of Eq. (A5) when correspondingly transformed.

APPENDIX B: CORRECTIONS DUE TO THE FINITE BANDWIDTH

The self-energy contribution Σ^D can be written a sum

$$\Sigma^D(z) = \Sigma_N^D(z) + \Sigma_S^D(z), \quad (B1)$$

where Σ_N^D is the contribution of just the normal lead and Σ_S^D is the same due to the superconducting leads:

$$\Sigma_N^D(z) = \sum_{\mathbf{k}} \mathbb{V}_{N\mathbf{k}}(z \cdot \mathbb{1} - \mathbb{E}_{N\mathbf{k}})^{-1}\mathbb{V}_{N\mathbf{k}},$$

$$\Sigma_S^D(z) = \sum_{\alpha \in \{L,R\},\mathbf{k}} \mathbb{V}_{\alpha\mathbf{k}}(z \cdot \mathbb{1} - \mathbb{E}_{\alpha\mathbf{k}})^{-1}\mathbb{V}_{\alpha\mathbf{k}}, \quad (B2)$$

with z being an arbitrary complex number. Later, only the functional form infinitesimally close to the real axis needs to be resolved. For that we set $z = \omega^+ \equiv \omega + i\eta$ with ω being a real frequency and η being an infinitesimally small positive number, thus taking the cut slightly above the real axis. The self-energy contribution $\Sigma_N^D(\omega^+)$ for the constant TDOS within the band (4) simply reads

$$\Sigma_N^D(\omega^+) = -i\Gamma_N\mathbb{1}, \text{ for } |\omega| < B. \quad (B3)$$

The superconducting part is nontrivial and shall be treated here in more detail. It is defined as

$$\Sigma_S^D(\omega^+) = \sum_{\alpha \in \{L,R\}\mathbf{k}} \mathbb{V}_{\alpha\mathbf{k}}(\omega^+\mathbb{1} - \mathbb{E}_{\alpha\mathbf{k}})^{-1}\mathbb{V}_{\alpha\mathbf{k}}, \quad (B4)$$

with notation following Sec. II B. The inverse matrix appearing in Eq. (B4) is evaluated using the identity $(u\mathbb{1} + \vec{v} \cdot \vec{\sigma})^{-1} = (u\mathbb{1} - \vec{v} \cdot \vec{\sigma})/(u^2 - \vec{v} \cdot \vec{v})$ as

$$(\omega^+\mathbb{1} - \mathbb{E}_{\alpha\mathbf{k}})^{-1} = \frac{\omega\mathbb{1} - \Delta C_\alpha\sigma_x + \Delta S_\alpha\sigma_y + \varepsilon_{\mathbf{k}\alpha}\sigma_z}{(\omega + i\eta)^2 - \Delta^2 - \varepsilon_{\mathbf{k}\alpha}^2}. \quad (B5)$$

Furthermore, since $\sigma_z(u\mathbb{1} + v_x\sigma_x + v_y\sigma_y + v_z\sigma_z)\sigma_z = u\mathbb{1} - v_x\sigma_x - v_y\sigma_y + v_z\sigma_z$, we get

$$\mathbb{V}_{\alpha\mathbf{k}}(\omega^+\mathbb{1} - \mathbb{E}_{\alpha\mathbf{k}})^{-1}\mathbb{V}_{\alpha\mathbf{k}} = V_{\alpha\mathbf{k}}^2 \frac{\omega\mathbb{1} + \Delta C_\alpha\sigma_x - \Delta S_\alpha\sigma_y + \varepsilon_{\mathbf{k}\alpha}\sigma_z}{\omega^2 - \Delta^2 - \varepsilon_{\mathbf{k}\alpha}^2 + i\eta\,\text{sgn}(\omega)},$$
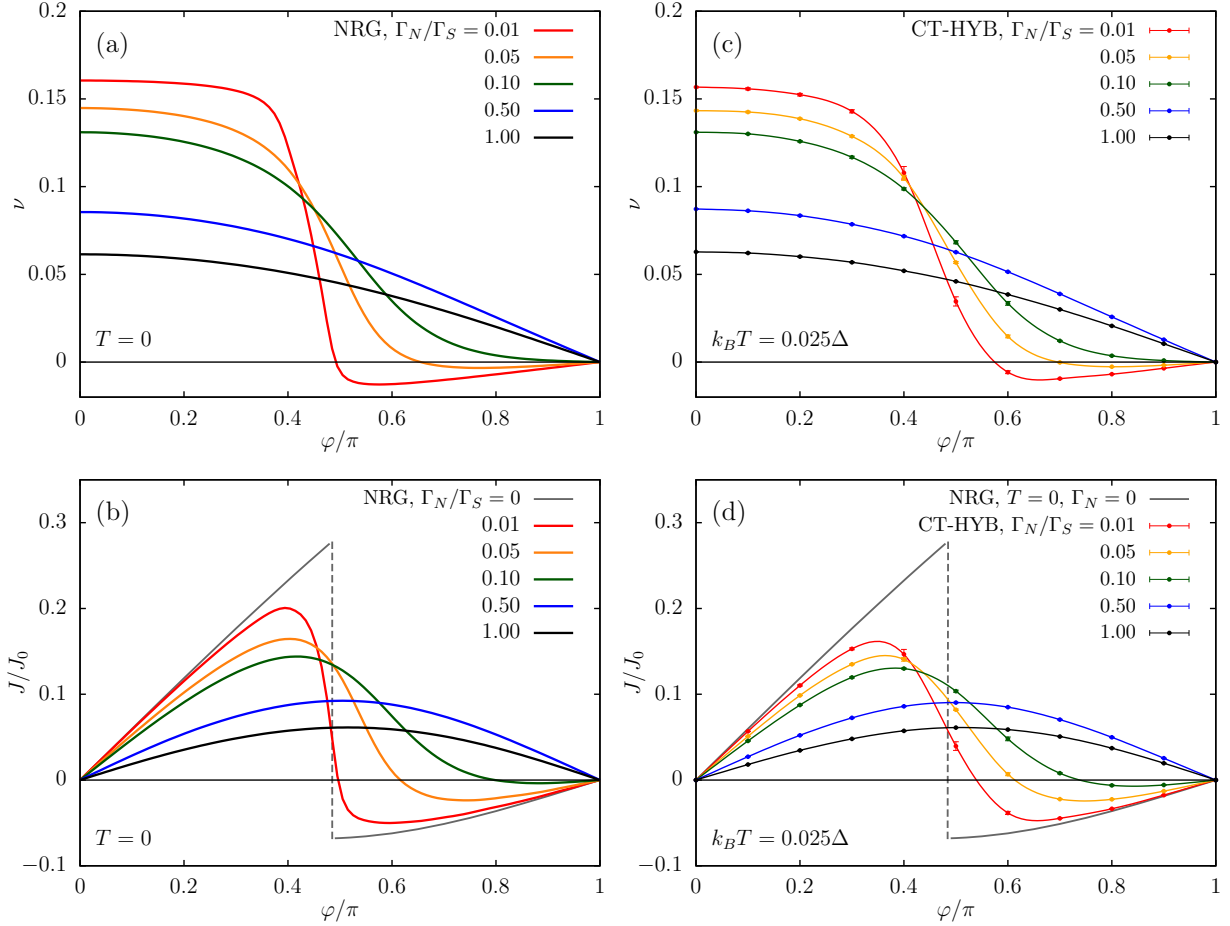
$$(B6)$$

FIG. 9. Left column: Phase-dependent on-dot pairing $\nu \equiv \langle d_\downarrow d_\uparrow \rangle$ (a) and the Josephson current J with $J_0 = 2e\Delta/\hbar$ (b) calculated using NRG at zero temperature in the w fields with subsequent use of Eqs. (42) and (43) for the parameters $B = 100\Delta$, $U = 3\Delta$, and $\Gamma_S = \Delta$ and various values of Γ_N. Right column: Equivalent results calculated using CT-HYB QMC in the basis of the d fields for small finite temperature $k_B T = \Delta/40$ (symbols with error bars): On-dot pairing ν (c) and Josephson current J (d). Lines are splines of QMC data and serve only as a guide to the eye.

which, eventually, under the assumption (4) of constant TDOS within the band leads to

$$\Sigma_S^D(\omega^+) = \sum_{\alpha \in \{L,R\}} \frac{\Gamma_\alpha}{\pi} \int_{-B}^{B} \frac{\omega \mathbb{1} + \Delta C_\alpha \sigma_x - \Delta S_\alpha \sigma_y}{\omega^2 - \Delta^2 - \varepsilon^2 + i\eta \, \text{sgn}(\omega)} d\varepsilon,$$

(B7)

where the term proportional to σ_z vanished due to the integrand being an odd function of ε. Using the symmetric phase drop gauge choice (cf. the discussion in Sec. II A) $\varphi_L = -\varphi_R = \varphi/2$, we sum over $\alpha \in \{L, R\}$ yielding

$$\Sigma_S^D(\omega^+) = \Gamma_S \left[\omega \mathbb{1} + \Delta \cos\left(\frac{\varphi}{2}\right) \sigma_x \right] F(\omega^+),$$

(B8)

with

$$F(\omega^+) \equiv \frac{1}{\pi} \int_{-B}^{B} \frac{d\varepsilon}{\omega^2 - \Delta^2 - \varepsilon^2 + i\eta \, \text{sgn}(\omega)}$$

$$= \frac{1}{\pi \sqrt{(\omega + i\eta)^2 - \Delta^2}} \ln \frac{\sqrt{(\omega + i\eta)^2 - \Delta^2} + B}{\sqrt{(\omega + i\eta)^2 - \Delta^2} - B}.$$

(B9)

Taking the $\eta \to 0$ limit, we arrive at

$$F(\omega^+) = \begin{cases} -\frac{2}{\pi \sqrt{\Delta^2 - \omega^2}} \arctan\left(\frac{B}{\sqrt{\Delta^2 - \omega^2}}\right), & \text{for } |\omega| < \Delta, \\ -\frac{i \, \text{sgn}(\omega)}{\sqrt{\omega^2 - \Delta^2}} + \frac{\ln\left(\frac{B + \sqrt{\omega^2 - \Delta^2}}{B - \sqrt{\omega^2 - \Delta^2}}\right)}{\pi \sqrt{\omega^2 - \Delta^2}}, & \text{for } \Delta < |\omega| < B. \end{cases}$$

(B10)

The resulting $\Sigma_S^D(\omega^+)$ has thus a nonzero imaginary part only outside of the gap region while all effects of the finite-sized band appear in its real part which is nonzero in the whole band. However, once the limit $B \to \infty$ is taken the real part out of the gap vanishes, too.

Altogether, the self-energy contribution $\Sigma^D(\omega^+)$ takes the form of Eq. (27), where

$$\Sigma_n^D(\omega^+) = -i\Gamma_N + \Gamma_S \omega F(\omega^+),$$

(B11)

$$\Sigma_a^D(\omega^+) = \Gamma_S \Delta \cos\left(\frac{\varphi}{2}\right) F(\omega^+).$$

(B12)

APPENDIX C: COMPARISON OF THE NRG RESULTS WITH QMC

In order to assess the ability of the presented NRG scheme to provide reliable results on the integral quantities like the

on-dot induced pairing and the Josephson current, we compare the results with a numerically exact CT-HYB QMC, as this method was already successfully used to study both the two-terminal [56] and three-terminal [34] setups and agrees with standard NRG results well within the QMC error bars.

The CT-HYB calculation is performed in the original d basis by employing the off-diagonal elements of the hybridization function using the TRIQS/CTHYB solver [57]. The total Hamiltonian of the system does not conserve particle number, therefore the superconducting pairing is introduced to the method using a canonical particle-hole transformation in the spin-down sector, mapping the system to an impurity Anderson model with attractive interaction [58,59]. As CT-HYB is an inherently finite-temperature method, all calculations were performed at $k_B T = \Delta/40$. All results are calculated for half-bandwidth $B = 100\Delta$ and a cutoff in Matsubara frequencies $\omega_n^{\max} \approx 314\Delta$.

The comparison of the NRG results with CT-HYB method is plotted in Fig. 9. In panel a (top left), NRG results for the induced pairing ν as a function of phase difference φ for $B = 100\Delta$, $U = 3\Delta$, $\Gamma_S = \Delta$ and various values of Γ_N at $T = 0$ are plotted. The importance of the finite-bandwidth corrections were already discussed in Fig. 8. The equivalent results of CT-HYB for small finite temperature are plotted in Fig. 8(c). The curves match within QMC error bars for small and large values of φ. In the crossover region, the results slightly differ as the finite temperature is a source of additional smearing, having a similar effect as Γ_N [34]. In Fig. 8(b) we plotted the NRG results for the Josephson current for the same set of parameters as in Fig. 8(a). We added a $\Gamma_N = 0$ result from Ref. [34] to mark the position of the QPT in a case of detached normal electrode. The relevant CT-HYB result is again plotted in Fig. 8(d). Comparison again shows good agreement up to the finite-temperature effects.

[1] S. J. Tans, M. H. Devoret, H. Dai, A. Thess, R. E. Smalley, L. J. Geerligs, and C. Dekker, Nature **386**, 474 (1997).

[2] A. Y. Kasumov, R. Deblock, M. Kociak, B. Reulet, H. Bouchiat, I. I. Khodos, Y. B. Gorbatov, V. T. Volkov, C. Journet, and M. Burghard, Science **284**, 1508 (1999).

[3] P. Jarillo-Herrero, J. A. van Dam, and L. P. Kouwenhoven, Nature **439**, 953 (2006).

[4] H. I. Jørgensen, K. Grove-Rasmussen, T. Novotný, K. Flensberg, and P. E. Lindelof, Phys. Rev. Lett. **96**, 207003 (2006).

[5] J. P. Cleuziou, W. Wernsdorfer, V. Bouchiat, T. Ondarcuhu, and M. Monthioux, Nat. Nanotechnol. **1**, 53 (2006).

[6] A. Eichler, R. Deblock, M. Weiss, C. Karrasch, V. Meden, C. Schönenberger, and H. Bouchiat, Phys. Rev. B **79**, 161407(R) (2009).

[7] J.-D. Pillet, C. H. L. Quay, P. Morfin, C. Bena, A. L. Yeyati, and P. Joyez, Nat. Phys. **6**, 965 (2010).

[8] R. Maurand, T. Meng, E. Bonet, S. Florens, L. Marty, and W. Wernsdorfer, Phys. Rev. X **2**, 011009 (2012).

[9] J. D. Pillet, P. Joyez, R. Žitko, and M. F. Goffman, Phys. Rev. B **88**, 045101 (2013).

[10] R. Delagrange, D. J. Luitz, R. Weil, A. Kasumov, V. Meden, H. Bouchiat, and R. Deblock, Phys. Rev. B **91**, 241401(R) (2015).

[11] J. A. van Dam, Y. V. Nazarov, E. P. A. M. Bakkers, S. De Franceschi, and L. P. Kouwenhoven, Nature **442**, 667 (2006).

[12] E. J. H. Lee, X. Jiang, R. Aguado, G. Katsaros, C. M. Lieber, and S. De Franceschi, Phys. Rev. Lett. **109**, 186802 (2012).

[13] E. J. H. Lee, X. Jiang, R. Žitko, R. Aguado, C. M. Lieber, and S. De Franceschi, Phys. Rev. B **95**, 180502(R) (2017).

[14] S. Li, N. Kang, P. Caroff, and H. Q. Xu, Phys. Rev. B **95**, 014515 (2017).

[15] A. C. Hewson, *The Kondo Problem to Heavy Fermions*, Cambridge Studies in Magnetism (Cambridge University Press, Cambridge, UK, 1993).

[16] K. G. Wilson, Rev. Mod. Phys. **47**, 773 (1975).

[17] P. Kopietz, L. Bartosch, and F. Schütz, *Introduction to the Functional Renormalization Group*, Lecture Notes in Physics (Springer-Verlag, Berlin, 2010).

[18] S. Streib, A. Isidori, and P. Kopietz, Phys. Rev. B **87**, 201107(R) (2013).

[19] K. Edwards, A. C. Hewson, and V. Pandis, Phys. Rev. B **87**, 165128 (2013).

[20] V. Janiš and P. Augustinský, Phys. Rev. B **75**, 165108 (2007).

[21] M. R. Buitelaar, T. Nussbaumer, and C. Schönenberger, Phys. Rev. Lett. **89**, 256801 (2002).

[22] A. Eichler, M. Weiss, S. Oberholzer, C. Schönenberger, A. Levy Yeyati, J. C. Cuevas, and A. Martín-Rodero, Phys. Rev. Lett. **99**, 126602 (2007).

[23] T. Sand-Jespersen, J. Paaske, B. M. Andersen, K. Grove-Rasmussen, H. I. Jørgensen, M. Aagesen, C. B. Sørensen, P. E. Lindelof, K. Flensberg, and J. Nygård, Phys. Rev. Lett. **99**, 126603 (2007).

[24] C. Buizert, A. Oiwa, K. Shibata, K. Hirakawa, and S. Tarucha, Phys. Rev. Lett. **99**, 136806 (2007).

[25] K. Grove-Rasmussen, H. I. Jørgensen, and P. E. Lindelof, New J. Phys. **9**, 124 (2007).

[26] D. J. Luitz, F. F. Assaad, T. Novotný, C. Karrasch, and V. Meden, Phys. Rev. Lett. **108**, 227001 (2012).

[27] A. Martín-Rodero and A. Levy Yeyati, Adv. Phys. **60**, 899 (2011).

[28] V. Meden, J. Phys.: Condens. Matter **31**, 163001 (2019).

[29] S. De Franceschi, L. Kouwenhoven, C. Schönenberger, and W. Wernsdorfer, Nat. Nanotechnol. **5**, 703 (2010).

[30] H. I. Jørgensen, T. Novotný, K. Grove-Rasmussen, K. Flensberg, and P. E. Lindelof, Nano Lett. **7**, 2441 (2007).

[31] R. Žitko, J. S. Lim, R. López, and R. Aguado, Phys. Rev. B **91**, 045441 (2015).

[32] G. Kiršanskas, M. Goldstein, K. Flensberg, L. I. Glazman, and J. Paaske, Phys. Rev. B **92**, 235422 (2015).

[33] A. Jellinggaard, K. Grove-Rasmussen, M. H. Madsen, and J. Nygård, Phys. Rev. B **94**, 064520 (2016).

[34] T. Domański, M. Žonda, V. Pokorný, G. Górski, V. Janiš, and T. Novotný, Phys. Rev. B **95**, 045104 (2017).

[35] K. Satori, H. Shiba, O. Sakai, and Y. Shimizu, J. Phys. Soc. Jpn. **61**, 3239 (1992).

[36] T. Yoshioka and Y. Ohashi, J. Phys. Soc. Jpn. **69**, 1812 (2000).

[37] Y. Tanaka, A. Oguri, and A. C. Hewson, New J. Phys. **9**, 115 (2007).

[38] A. Oguri and Y. Tanaka, J. Phys.: Conf. Ser. **391**, 012146 (2012).

[39] A. Oguri, Y. Tanaka, and J. Bauer, Phys. Rev. B **87**, 075432 (2013).

[40] R. Bulla, T. A. Costi, and T. Pruschke, Rev. Mod. Phys. **80**, 395 (2008).

[41] J.-G. Liu, D. Wang, and Q.-H. Wang, Phys. Rev. B **93**, 035102 (2016).

[42] In the present model, half-filling implies that the system is tuned to the particle-hole symmetric point, see Ref. [37].

[43] R. Bulla, J. Keller, and T. Pruschke, Z. Phys. B Condens. Matter **94**, 195 (1994).

[44] T. Hecht, A. Weichselbaum, J. von Delft, and R. Bulla, J. Phys.: Cond. Mat. **20**, 275213 (2008).

[45] R. Žitko, NRG Ljubljana—Open source numerical renormalization group code (2014).

[46] A. Kadlecová, M. Žonda, and T. Novotný, Phys. Rev. B **95**, 195114 (2017).

[47] The argument ω^+ of the function emphasizes to which part of the complex z plain it belongs (above vs. below the real axis of z). This notation is employed throughout this paper when required.

[48] T. Novotný, A. Rossini, and K. Flensberg, Phys. Rev. B **72**, 224502 (2005).

[49] The spectral functions have been obtained using the open source NRG Ljubljana code [45] in the one-channel mode with intertwined z discretization [51] with $z = n/10$, $n \in \{0, \ldots, 10\}$.

[50] The broadening has been also predicted analytically in Refs. [34,53] via the Schrieffer-Wolff transformation. Using the transformation $\mathbb{T}$, the $\Delta \to \infty$ can be mapped onto the particle-hole asymmetric SIAM, from which the enhancement of the exchange coupling J compared to the particle-hole symmetric case follows trivially. Thus, as a consequence of the locally induced SC pairing, the T_K is enhanced and the central peak is broader compared to the single-channel normal SIAM.

[51] R. Žitko and T. Pruschke, Phys. Rev. B **79**, 085106 (2009).

[52] M. Žonda, V. Pokorný, V. Janiš, and T. Novotný, Sci. Rep. **5**, 8821 (2015).

[53] T. Domański, I. Weymann, M. Barańska, and G. Górski, Sci. Rep. **6**, 23336 (2016).

[54] R. Fazio and R. Raimondi, Phys. Rev. Lett. **80**, 2913 (1998).

[55] A. K. Mitchell, M. R. Galpin, S. Wilson-Fletcher, D. E. Logan, and R. Bulla, Phys. Rev. B **89**, 121105(R) (2014).

[56] A. Kadlecová, M. Žonda, V. Pokorný, and T. Novotný, Phys. Rev. Appl. **11**, 044094 (2019).

[57] P. Seth, I. Krivenko, M. Ferrero, and O. Parcollet, Comput. Phys. Commun. **200**, 274 (2016).

[58] D. J. Luitz and F. F. Assaad, Phys. Rev. B **81**, 024509 (2010).

[59] V. Pokorný and M. Žonda, Physica B **536**, 488 (2018).